Research Square

Preprints are preliminary reports that have not undergone peer review.
They should not be considered conclusive, used to inform clinical practice,
or referenced by the media as validated information.

Application of kilohertz-frequency block to mitigate off-target motor effects of vagus nerve stimulation in swine

Kip Ludwig

kaludwig2@wisc.edu

University of Wisconsin - Madison

Kevin Cheng

University of Wisconsin-Madison https://orcid.org/0000-0002-8078-2158

Ashlesha Deshmukh

University of Wisconsin-Madison

Aaron Gholston

University of Wisconsin-Madison

Megan Settell

University of Wisconsin-Madison

Bruce Knudsen

Mayo Clinic

Maria LaLuzerne

University of Wisconsin-Madison

James Trevathan

University of Wisconsin-Madison https://orcid.org/0000-0002-7282-4872

Aaron Suminski

University of Wisconsin–Madison https://orcid.org/0000-0002-8793-5049

Nicole Pelot

Duke University https://orcid.org/0000-0003-2844-0190

Warren Grill

Duke University https://orcid.org/0000-0001-5240-6588

Article

Keywords:

Posted Date: April 14th, 2025

DOI: https://doi.org/10.21203/rs.3.rs-6378942/v1

License: This work is licensed under a Creative Commons Attribution 4.0 International License.
Read Full License

Additional Declarations:
Yes there is potential Competing Interest. Nature Disclosure of Potential Competing Interest document included with uploaded files.

The authors declare the following competing interests: KAL is a co-founder and equity holder of NeuraWorx. KAL is a scientific board member and has stock interests in NeuroOne Medical Inc. KAL is also a paid member of the scientific advisory board of Abbott and Presidio Medical, and a paid consultant for HuMANNity, ONWARD and Restora Medical. WMG is an inventor on licensed patents on waveforms for neural block and receives associated royalty payments. KPC is a paid consultant of Neuraworx. JKT is a paid consultant for Presidio Medical, Inc. The remaining authors declare that the research was conducted in the absence of any additional commercial or financial relationships that could be construed as a potential conflict of interest.

Version of Record: A version of this preprint was published at Nature Communications on December 30th, 2025. See the published version at https://doi.org/10.1038/s41467-025-67823-0.

Application of kilohertz-frequency block to mitigate off-target motor effects of vagus nerve stimulation in swine

Kevin P. Cheng[1,2], Ashlesha Deshmukh[2,3], Aaron K. Gholston[2,3], Megan L. Settell[1-3], Bruce E. Knudsen[1,2], Maria LaLuzerne[1,2], James K. Trevathan[1-3], Aaron J. Suminski[1,2], Nicole A. Pelot[5], Warren M. Grill[5], Kip A. Ludwig[1-4,]

*Corresponding Author Contact:
Dr. Kip Ludwig, PhD
Associate Professor, Departments of Neurological Surgery and Surgery
Co-Director, Wisconsin Institute for Translational Neuroengineering (WITNe)
Kip.Ludwig@wisc.edu
608 265 3544

[1] Department of Neurological Surgery, University of Wisconsin – Madison, WI
[2] Wisconsin Institute for Translational Neuroengineering (WITNe), University of Wisconsin – Madison, WI
[3] Department of Biomedical Engineering, University of Wisconsin-Madison, Madison, WI
[4] Department of Surgery, University of Wisconsin-Madison, Madison, WI
[5] Department of Biomedical Engineering, Duke University, Durham, NC

ABSTRACT

Selective activation of smaller diameter over large diameter nerve fibers represents a broad challenge in the electrical modulation of neural activity for clinical applications. For example, off-target activation of motor nerve fibers has been implicated in several failed vagus nerve stimulation (VNS) clinical trials by precluding achieving current amplitudes sufficient to activate the therapeutically targeted small diameter fibers. In this study, we evaluated the use of high-frequency (HF) stimulation to block unwanted activation of large diameter fibers evoked by traditional low-frequency (LF) VNS in a large animal (swine) model. We demonstrate that HF can eliminate specific unwanted LF-evoked components from neural recordings with high selectivity – along with their associated off-target physiological responses - while preserving the activation of smaller diameter fibers driving intended physiological responses. Conversely, block of the smaller diameter fibers was only observed at HF amplitudes much higher than amplitudes commonly used for HF block clinically. We found that in addition to blocking the LF-evoked compound action potential, lower HF amplitudes also drive asynchronous activity which can easily be overlooked. Only at high amplitudes did HF block LF-evoked activation without concomitant asynchronous activation. These data have numerous implications for existing and future LF and HF block neuromodulation therapies.

INTRODUCTION

Electrical modulation of neural activity, also known as bioelectronic medicine or electroceuticals, is a rapidly growing medical device sector with applications across a broad spectrum of conditions[1–3]. For example, vagus nerve stimulation (VNS), which is FDA-approved for the treatment of depression, epilepsy, obesity, and stroke after-effects, is also being investigated to treat heart failure, diabetes, and chronic inflammatory diseases[4–10]. The range of clinical applications of VNS reflects the breadth and complexity of the anatomy of the vagus nerve (VN) with afferent pathways conveying sensory information from the viscera and efferent pathways exerting autonomic influence on many end organs[11–13]. However, the VN is a mixed nerve which also contains somatic motor efferents[11,14–16]; these large-diameter myelinated motor A-alpha (m-Aα) nerve fibers innervate muscles of the neck, and are activated at lower stimulation amplitudes than the smaller diameter A-delta (Aδ) sensory afferents and parasympathetic B-fibers targeted for most VNS indications[15–19]. This relationship between fiber diameter, function, and activation threshold highlights a broader challenge in neuromodulation: activation of off-target large-diameter m-Aα fibers frequently limits the stimulation amplitude that can be applied in bioelectronic medicine due to unwanted, sometimes painful, side effects[15,20–22].

Experimental and computational modeling studies—spanning rodents, dogs, pigs, and humans—show that thresholds for activation of vagal m-Aα fibers are ~1/5th of the amplitudes needed to activate small-diameter therapeutic fibers[15,16,18,19,23]. Thus, current VNS clinical practice for epilepsy requires a months-long process to habituate patients to the m-Aα activation by incrementally increasing the applied VNS current, which typically plateaus at a 'therapeutic dose' of 1.5 – 2.25 mA[20]. Unfortunately, these amplitudes are still insufficient to activate all but the most superficial Aδ/B fibers, and may not activate any therapeutic target fibers in some patients depending on subject-to-subject variations in vagal anatomy[15,16,18,19,24]. As a result, therapy-limiting side effects were implicated in a host of recent failed VNS clinical trials, despite promising results in animal models[25]. For example, in the NECTAR pivotal trial of VNS to treat heart failure, it was reported that only 12% of patients exhibited the stimulation-induced changes in heart rate (HR) mediated by activation of parasympathetic B-fibers[22]. Off-target neck muscle activation was the most commonly cited reason for limiting the VNS current, resulting in amplitudes at or beneath the threshold for activating B-fibers in large animal models[15,19–22].

Several strategies have been proposed to reverse the conventional order of stimulation recruitment and achieve activation of therapeutically-targeted small diameter fibers without activation of side-effect generating large diameter fibers[16,21,22,26–42]. Spatially selective cuff electrode designs aim to exploit somatotopy of the VN by positioning small electrode contacts close to the therapeutic target fibers and far from fibers that cause side-effects. However, individual anatomical variability may limit the effectiveness of this strategy[14,24,29,40,41]. Novel stimulation waveforms can achieve selective activation of small diameter fibers, such as anodal block, depolarizing pre-pulses, slowly rising ramp pulses, and very low-frequency (LF) sinusoids [26,31,34,35,43–46]. While some approaches narrowed the difference in activation thresholds between m-Aα and smaller diameter therapeutic fibers, none has shown a sufficiently large effect to overcome the ~5X threshold difference needed to activate smaller fibers before m-Aα's.

High-frequency (HF) waveforms (>5 kHz) have recently received increased attention for therapeutic applications. With appropriate waveform parameters, HF signals can block propagating action potentials (APs)[47–57], and larger diameter fibers are blocked at lower amplitudes than smaller diameter fibers[51,52,55,58]. The feasibility of using solely HF signals to selectively activate small diameter fibers while blocking large diameter fibers was recently demonstrated in a rodent model[42]. However, it is unclear whether similar results are possible in a more clinically relevant large animal model, with a thicker epineurium, multi-fascicular nerve morphology, a greater range of electrode-fiber distances, more numerous nerve fibers, and larger electrodes. Moreover, the asynchronous activation of nerve fibers by HF signals, and its clinical applicability, is less understood as compared to traditional LF stimulation[48,52–55,58].This creates a large unknown variable in appropriate tuning of HF to achieve desired clinical effects when compared to LF stimulation where a large body of pre-clinical and clinical data establishing stimulation parameters, safety, and efficacy already exists[25].

We evaluated whether HF signals layered onto standard low-frequency VNS (LF-VNS) could selectively block m-Aα fibers to achieve net selective activation of small diameter fibers. We measured the evoked neural, muscular, and cardiac responses to traditional LF-VNS while applying a 10 kHz HF signal at varying amplitudes. We demonstrate that increasing HF amplitudes can selectively block components of the LF-VNS evoked compound action potential (eCAP), following the order of recruitment from larger to smaller diameter fibers. After establishing selectivity, we then evaluate the HF dosing that blocks LF-VNS-evoked small fiber activity and associated HR responses. Importantly, we establish that the HF amplitude can be titrated to eliminate LF-VNS-evoked motor side-effects while preserving activation of smaller diameter fibers and their consequent effects on HR in a mixed nerve with a size and fascicular organization comparable to humans[14,24].

RESULTS

10 kHz HF blocks VNS-evoked motor side effects

We applied cervical LF-VNS while measuring the evoked electromyogram from the cricoarytenoid neck muscles (EMG_{CA}) to assess the effects of a 10 kHz sinusoidal HF signal on LF-VNS motor side effects (Figure 1A). The HF signal was applied through a separate cuff located distally to the LF-VNS cuff. Each trial was sub-divided into three periods: pre-HF to assess the physiologic effects of LF-VNS alone, LF-VNS + 10 kHz HF to assess the effects of HF on the LF-VNS-evoked responses, and post-HF to assess how the LF-VNS-evoked responses recovered following cessation of HF (Figure 1B). Figure 1C shows example EMG_{CA} responses to LF-VNS with increasing HF current amplitude.

HF blocked the LF-VNS-evoked muscle activity in an amplitude-dependent manner, and increasing HF caused partial and then complete block of the evoked EMG_{CA} (Figure 1C-F). To generate HF dose-response curves (DRCs), we calculated the root-mean-squared of the EMG_{CA} (V_{rms}) for the pre-HF and during-HF periods; to account for surgical and subject differences, EMG_{CA} values were normalized ($\tilde{V}_{rms}$) within trial by the pre-HF EMG_{CA} V_{rms}. Low HF amplitudes (0.5 mA) generated little to no block of the LF-VNS-evoked muscle activity (HF = 0.5 mA, $\tilde{V}_{rms}$ = 101.1 ± 1.4%, mean ± 1 standard error of mean (s.e.m.)). Intermediate HF amplitudes (HF = 1-3 mA) elicited partial block of EMG_{CA} ($\tilde{V}_{rms}$ = 65.4 ± 13.9%, 39.1 ± 17.1%, 10.7 ± 6.4 @ 1, 2, 3 mA respectively), which tended to recover in amplitude over time, but did not return to the full amplitude EMG_{CA} within the 30-second HF period (Figure 1D, Supplemental Figure 6). As the HF amplitude was increased >4 mA, we observed near total block of the evoked EMG_{CA} (HF = 4 mA, $\tilde{V}_{rms}$ = 3.6 ± 1.7%). The dramatic reduction in EMG and small variance across subjects (n=5) at 4 mA HF and beyond suggest that this amplitude was sufficient to block nearly all m-Aα's within the cervical VN regardless of anatomical differences. We also confirmed that the HF signal generated local conduction block of fibers within the HF cuff as the HF signal did not block EMG_{CA} when LF-VNS was applied caudally to the HF cuff nor did the HF signal block the EMG evoked by current escape from the LF-VNS cuff to the superior laryngeal (SL) nerve (Supplemental Figures 1 & 2).

Titrating HF amplitude blocks individual eCAP components

The goal of HF signals in clinical applications is to block activation of m-Aα's without blocking smaller therapeutic target fibers. After establishing that HF could block EMG_{CA} responses, we next sought to determine whether the progressive increase in thresholds to block smaller diameter nerve fibers in rodents[51,52,55,56,58] could also be achieved in a mixed nerve of comparable size to the human vagus.

Longer latency components of LF-VNS eCAPS (i.e., from smaller diameter fibers) were blocked at higher HF amplitudes than shorter latency components. We consistently observed at least three eCAP components, depending on the amplitude of LF-VNS (Figure 2), and confirmed their neural origin using a muscle paralytic (Supplemental Figure 3). At 1 mA LF-VNS, two eCAP components were present accompanied by an EMG artifact that occurred ~8 ms after the LF-VNS pulse (Figure 2A) whereas the 3rd eCAP component was only present at higher LF-VNS amplitudes (Figure 2B). These components can be categorized into m-Aα/Aβ (Component 1, CV ≈ 43 m/s, red-shaded region), Aγ/Aδ (Component 2, CV ≈ 25 m/s, blue-shaded region), and slower Aδ-delta/B-fibers (Component 3, CV ≈ 10 m/s, green-shaded region) based on the Erlanger-Gasser scale[15,59–63].

The presence of EMG contamination in eCAP recordings can make interpretation of longer-latency eCAP components difficult as the EMG contamination may be mistaken for (e.g. Figure 2A dashed box) or distort the long-latency, slower (small fiber), neural eCAP, (e.g. Figure 2B, Component 3 at HF = 0 mA)[15,16]. When the LF-VNS amplitude was increased to activate smaller diameter fibers and HF amplitude was above the complete EMG_{CA} block threshold, elimination of the EMG artifact provided clear identification of eCAP Component 3 (Figure 2A, B dashed boxes). Component 3 had a conduction velocity consistent with activation of Aδ/B fibers, i.e., the intended target for most VNS therapies. In addition, we took two approaches to confirm that the analyzed eCAP signals were neural in origin rather than being confounded by EMG artifacts. First, we repeated a subset of eCAP recordings with a paralytic to confirm the neural origin of Component 3 and its attenuation by high amplitude HF (n = 3/5 subjects, Supplemental Figure 3). Second, as expected, the distally applied HF signal did not block EMG activated by current escape from the LF-VNS cuff caudally to the SL-nerve (Supplemental Figure 2). Thus, we excluded subjects (P01,P04) and LF-VNS amplitudes that evoked a secondary short-latency EMG in the analysis of eCAP Component 3.

Each of the eCAP components was affected by the HF signal at different amplitudes in a latency-dependent—and therefore fiber size-dependent—manner from larger to smaller diameter fibers (Figure 2, Supplemental Figures 4 for individual responses). Component 1 (Figure 2A, red-shaded region) was significantly attenuated at HF amplitudes ≥2 mA ($\tilde{V}_{rms}$ = 45 ± 6.4%, p=0.007), Component 2 (Figure 2A, blue-shaded region) was significantly attenuated at HF amplitudes ≥4 mA ($\tilde{V}_{rms}$ = 45.3 ± 10.6%, p=0.007), and Component 3 (Figure 2B, green-shaded region) was significantly attenuated at HF amplitudes ≥15 mA ($\tilde{V}_{rms}$ = 26.7 ± 5.4%, p=0.003). Thus, HF can be titrated to block specific fiber diameters while leaving the next largest fibers largely unaffected until increased amplitudes of HF amplitude are applied.

The coincident changes in the EMG_{CA} response and Component 1 of the eCAP as HF amplitude was increased suggested that this component of the eCAP reflected activation (and block) of m-Aα nerve fibers responsible for therapy-limiting side-effects in clinical VNS (Figure 3A red-shaded region and 3B gray-shaded region). This was supported by the strong correlation between the 1st eCAP component and the LF-VNS evoked EMG_{CA} response (Spearman's R=0.95, Figure 3C). Conversely, the 2nd eCAP component correlated poorly with the EMG_{CA} response (Spearman's R=0.46, Figure 3D) and may represent intermediate diameter vagal afferents.

Onset EMG effects scale with HF amplitude

The effect of HF on an individual nerve fiber is dependent on the strength of the HF electric field; at lower amplitudes, HF induces a transient onset response and can evoke sustained (albeit asynchronous) activation at amplitudes less than required to produce block[49,51,54,55,64]. Therefore, within a given nerve with different fiber diameters and electrode-fiber distances, some fibers may be blocked, while others may be in an activated (sub-block) state. Because HF evokes asynchronous activity, we examined these activation responses by generating color-coded pulse-by-pulse raster plots of the EMG_{CA} during HF that depict the combined LF-VNS-evoked and HF-evoked EMG_{CA} responses during a trial (Figure 4A, B; see Supplemental Figure 5 for explanation of raster plot generation).

In all applications of HF, the EMG_{CA} showed an immediate onset response (Figure 4A green arrowheads, Figure 4B onset spikes) at the initiation of HF. Depending on the HF amplitude, this onset response was accompanied by asynchronous muscle activity (e.g. sporadic muscle twitches not synchronized with LF-VNS), indicative of sustained, asynchronous, m-Aα activation. We quantified the degree of HF-induced activity by the number of twitch responses evoked during the HF period (minus the LF-VNS-evoked EMG_{CA}; Figure 4C) and their relative magnitude in comparison to the LF-VNS-evoked EMG_{CA} (Figure 4D). This asynchronous activity generally diminished over the duration of HF at sub-block amplitudes (Figure 4A, 1 and 2 mA HF, Supplemental Figure 6) and was less present at HF amplitudes that blocked the LF-VNS-evoked EMG_{CA} (Figure 4A, 4 and 20 mA HF). The number of muscle twitches decreased as the HF amplitude was increased (Figure 4C) whereas their relative magnitude was consistently ~20% of the LF-VNS (1 mA) evoked EMG_{CA} response regardless of the HF amplitude (Figure 4D, Kruskal-Wallis H=2.59, p = 0.62). The consistent magnitude of the asynchronous twitches may be explained by asynchronous activation of motor units by HF, in contrast with the

LF-VNS-evoked synchronous activation that results in temporal summation. Consistent with rodent studies, in a subset of subjects, we observed carryover effects of HF where the LF-VNS-evoked EMG_{CA} remained blocked or partially blocked beyond the HF period, albeit only at the highest HF amplitudes tested (Figure 4A, 20 mA)[49,65].

10 kHz HF effects on the LF-VNS cardiac response

Recent failed pivotal trials for VNS to treat heart failure demonstrate the necessity of developing methods to activate small diameter fibers selectively while blocking large diameter fibers responsible for limiting patients to sub-therapeutic doses[22,25,65–68]. We sought to determine whether m-Aαs can be blocked while preserving LF-VNS cardiac effects by assessing paired EMG_{CA} and cardiac responses to varying levels of LF-VNS and HF (Figure 5A, Supplemental Figure 7).

Low amplitudes of LF-VNS evoked tachycardia that transitioned to bradycardia at higher LF-VNS amplitudes (Figure 5A, top row)[69]. When lower amplitude HF (but still above EMG_{CA} block threshold, Figure 1) was also applied, no changes in cardiac effects were observed at any LF-VNS dose (Figure 5A, green) indicating that HF levels that blocked EMG_{CA} (i.e., m-Aαs) were insufficient to cause activation or block of the smaller diameter vagal cardiac B-fibers responsible for LF-VNS bradycardic effects. At 10 mA HF, a small onset bradycardia was observed at the initiation of HF in some trials as evidenced by the sharp change in HR during the first several seconds of HF (Figure 5A, yellow) which was stronger at 15 mA HF. This transient response is likely due to brief HF-induced onset activation of B-fibers in a manner similar to the onset EMG_{CA} activity (Figure 4A, B). When the LF-VNS current amplitude was high enough to evoke strong bradycardia (Figure 5A, right column), block of LF-VNS-evoked bradycardia only occurred at high levels of HF (Figure 5A, gray) with even higher levels of HF evoking more complete block of LF-VNS bradycardic effects (Figure 5B).

In contrast, the effects of HF on LF-VNS-evoked tachycardia (Figure 5A, left and middle columns) were more complex with some trials exhibiting apparent block whereas others only exhibited a transient bradycardic HF onset response. LF-VNS tachycardic effects are believed to be centrally mediated responses to vagal afferents with multiple effector pathways besides the VN[16,69]. Thus, application of HF caudal to the LF-VNS cuff, as in our experiment, would not be expected to block these effects. Instead, trials in which HF induced a sustained bradycardic effect during a LF-VNS tachycardic response (Figure 5A, 3 mA LF-VNS + 15 mA HF) may have been the result of HF-induced activation of parasympathetic cardiac B-fibers overriding the centrally mediated tachycardic effects.

We compared the 3rd component of the eCAP, whose conduction velocity was consistent with small Aδ/B-fibers, with the HR response to determine whether the HF effect on LF-VNS cardiac responses was reflected in the eCAP. However, the long inter-trial duration for washout, the high LF-VNS amplitudes required to evoke B-fiber mediated bradycardia, and the complexity of the HR responses precluded generation of dose response curves with sufficient resolution to correlate bradycardia to the amplitude of the Aδ/B-fiber eCAP components. Nonetheless, the amplitude of the 3rd eCAP component tracked well the effects of HF on LF-VNS-evoked bradycardia indicating that it may represent these small diameter vagal efferents (Supplemental Figure 8).

HF can selectively block LF-VNS-evoked EMG without influencing LF-VNS cardiac responses

Our results support the feasibility of titrating LF-VNS and HF amplitudes to eliminate EMG_{CA} responses (i.e., side effects of clinical VNS) while preserving LF-VNS-mediated changes in HR, including tachycardia (Figure 6A) and bradycardia (Figure 6B). Paired EMG_{CA} and HR responses demonstrate that 4 mA HF completely blocked EMG_{CA} and produced no effects on the LF-VNS cardiac response (Figure 6). In practice, this would enable higher amplitudes of LF-VNS to be applied clinically, as required for greater therapeutic effects, than would be possible without HF, where neck muscle activation limits the LF-VNS current level[15,19–22]. Only when HF amplitude was increased sufficiently (>10 mA) to interact with smaller diameter fibers were effects evident on LF-VNS evoked cardiac responses (Figure 6A, B).

An ‘HF-window’ was identified in all subjects (Figure 6C, light blue shaded region) where the LF-VNS EMG_{CA} was reduced to less than 20% of its pre-HF magnitude, while maintaining LF-VNS-evoked changes in

HR. HF amplitudes of 2.4 ± 0.24 mA blocked EMG_{CA}, whereas HF amplitudes of 10.2 ± 1.42 mA were required for HF-evoked changes in HR (see Supplemental Figure 7 for full cohort HF-windows). This approximately five-fold difference in thresholds is due to the fiber diameter selectivity of HF and suggests there is a dynamic range over which HF can be titrated to block the LF-VNS evoked EMG_{CA} without interfering with therapeutic cardiac effects. Note however that due to experimental time constraints, not all HF amplitudes within this range were tested (Figure 6C striped region), and it is possible that the HF window is smaller than reported here (i.e., on average, the highest HF amplitude tested that did not evoke any cardiac responses was 6.4 ± 2.19 mA).

DISCUSSION

This is the first comprehensive analysis of the potential utility of HF to selectively block nerve fibers within large-diameter mixed nerves like the human vagus. Prior studies of HF were predominantly conducted in rodents, where the combination of smaller electrodes, nerve bundles, and electrode-fiber distances result in larger transmembrane voltage changes at a given applied current in comparison to pig or human nerves[18,24,42,49,70–73]. The few HF studies in large animals largely focused on LF-evoked motor responses[74–78], which result from activation and/or block of large diameter m-Aα fibers that have 5-10x lower thresholds than the smaller diameter therapeutic fibers targeted for VNS therapies[15,16,18,42,60]. In this study, we assessed whether HF could be used in conjunction with LF-VNS to prevent conduction of neural activity in the side effect-producing m-Aα's in the pig large animal model, while leaving intact propagation in therapeutic smaller diameter fibers which form the basis for some clinical applications of VNS. Our data demonstrates that this can be achieved by 10 kHz HF with a high degree of selectivity for the fiber type blocked based on HF amplitude. Moreover, our results indicate that HF creates conduction block local to the HF cuff (Supplemental Figure 1, 2)—consistent with prior studies of HF block[79–81]—and would therefore not interfere with VNS therapies targeting afferent, centrally-mediated, effects (e.g., epilepsy, depression) while preventing motor associated side-effects. This opens the potential for greatly increasing current amplitude limits in clinical VNS by eliminating the primary constraint of neck muscle activation cited by multiple failed clinical trials[10,22,66,67].

HF signals putatively block conduction by generating rapid transmembrane voltage oscillations that are rectified by non-linear membrane properties to cause net depolarization and inactivation of sodium channels(i.e., comparable to the refractory period)[48,51,52]. The sustained average depolarization during the application of HF prevents repolarization and sodium channel de-inactivation, leaving them in the inactivated state[48,51,52,82]. Conduction block is created when a sufficient number of sodium channels within an axon segment are held in the inactivated state by the HF signal[51]. Thus, the effect of HF is dependent on the magnitude of transmembrane potential oscillations experienced by the axon which are, in turn, dependent on the fiber diameter, the distance from the HF electrode, the fascicular structure of the nerve (and associated tissue conductivities), and the HF signal frequency, waveform, and amplitude. When generating smaller transmembrane potential oscillations, HF evokes asynchronously occurring APs for the period it is applied as an insufficient number of sodium channels are inactivated to create block[42,49,51–53,55,64]. In contrast, when larger transmembrane potential oscillations are generated, HF will drive most sodium channels into the inactivated state thereby inhibiting or fully blocking the propagation of APs[42,49,51–53,55,83,84].

The graded block of LF-VNS EMG_{CA} as HF amplitude increased (Figure 1F) is consistent with lower HF block thresholds for m-Aα fibers closer to the HF electrode and higher block thresholds for m-Aα fibers further from the electrode (Figure 1F, >4 mA). The larger variance in the partial EMG_{CA} block responses at intermediate HF amplitudes (Figure 1F, 1-3 mA) may be due to differences in individual fascicular anatomy or fiber organization across subjects. This would change the relative distance of the EMG_{CA} evoking fibers from the HF cuff leading to differences in sensitivity to HF blocking effects until an HF amplitude is reached which blocks all m-Aα's regardless of position within the nerve.

In addition to its effects on LF-VNS-evoked EMG_{CA}, HF also generated asynchronous EMG_{CA} activity arising from the asynchronous APs generated by sub-block HF amplitudes[85]. While these asynchronous responses tended to diminish as the total EMG_{CA} block threshold was approached, they were often not eliminated until HF current levels higher than needed to achieve total block of the LF-VNS-evoked EMG_{CA} were reached. Further, there were trials in which the asynchronous activity was stronger at a higher HF amplitude

(see subject P05, Supplemental Figure 6), even after total block of the LF-VNS EMG_{CA} was achieved. This could be due to the higher than necessary HF amplitude activating fibers at the boundaries of the HF's electric field[55] and suggests that fine control should be maintained to minimize HF-evoked asynchronous activity while effectively blocking the LF-VNS evoked EMG. However, we also found that the magnitude of the asynchronous EMG_{CA} responses during HF were only ~20% the amplitude of the LF-VNS evoked response regardless of the HF amplitude (at 1mA LF-VNS, Figure 4D), which may indicate an absence of temporal summation of responses to asynchronous m-Aα activity. These smaller asynchronous responses may be somewhat inconsequential if they are within tolerable limits for patients undergoing the habituation process. However, as our subjects (anesthetized pigs) were unable to report on the off-target sensation produced by this asynchronous activity, it remains unclear whether the HF-evoked asynchronous activation would be as intolerable as the LF-VNS-evoked synchronous neck-muscle activation that has limited therapeutic current levels in clinical VNS. Similarly, the partial block that we observed at lower amplitudes of HF may itself be sufficient to facilitate higher clinical LF-VNS current amplitudes if partial block can diminish neck muscle activation to tolerable levels. This approach could conserve battery life by reducing power consumption and limit potential risks by using a lower HF amplitude while still enabling a higher applied current for therapeutic LF-VNS.

The mechanism of action noted above is most often associated with an onset response before entering a blocked state. Consistent with previous rodent studies[49,86,87], there was brief HF onset activation of m-Aα fibers prior to blocking in all trials (Figure 4B onset spikes). This onset response was comparable in size to the LF-VNS-evoked EMG_{CA} and may therefore limit the effective therapeutic range of HF, if the onset causes an intolerable (albeit brief) neck muscle activation. A number of strategies have been proposed for preventing this onset response including combined dc and kHz HF stimulation, ramping, or novel HF waveforms[50,54,83,88,89].

We analyzed HF onset from the EMG_{CA} but not eCAPs due to the inherently lower signal-to-noise ratio of eCAPs vs. EMG in comparison to the HF artifact. Further, classifying eCAP components based on latency would not be possible for asynchronous HF-induced eCAP signals. Nonetheless, our cardiac data indicate that smaller diameter fibers likely also exhibited some HF-generated onset as evidenced by the transient bradycardia observed at the initiation of HF (Figure 5A black arrowheads, Supplemental Figure 7). While the HF-induced EMG activity may be undesirable but ultimately innocuous muscle twitches, long-term asynchronous activity in other vagal fibers, for which there is no clear and measurable effector output, remain unknown and should be better understood before clinical implementation of HF in VNS therapy. This may be especially true in VNS applications where the intended goal is to modulate central activity, entrainment, and/or plasticity as the asynchronous HF induced APs may interfere with this effect[90–94].

Likewise, it remains unclear if persistent block of large diameter fibers within the cervical vagus could create unwanted side effects, including block of natural physiological traffic. In the case of m-Aα's, this may impair voluntary control of these muscles during the HF period and potentially cause chronic issues such as those observed in long-term denervation[95]. It could also lead to block of large diameter sensory afferents from the viscera if the HF amplitude is not appropriately titrated to leave their activity intact. Further, the long-term effects of HF on axonal homeostasis are poorly understood. Changes in sodium channel kinetics may result in compensatory changes in other voltage-gated ion channels, potentially impacting intracellular ion concentrations, and affecting the functions of the endoplasmic reticulum, mitochondria, and other organelles[96–99]. Thus, more in-depth and chronic studies should be performed profiling the genomic, transcriptomic, and proteomic effects of HF on individual nerve fibers that better capture its long-term effects[44,46,52].

Application of HF at the current levels needed to achieve block of large diameter fibers also has important instrumentation, electrochemical, and energy consumption issues to consider. In terms of instrumentation, inadequate control of direct current (dc) leakage can occur during HF signals, which may be responsible for inconsistent results between studies and could cause harmful electrochemical reactions[52,100]. In this study, a specialized dc blocking circuit was used to eliminate this problem[100]. Moreover, the existing paradigm to assess long-term electrochemical risks—the Shannon limit[101]—established guidelines derived from phenomenological studies that are only applicable to stimulation under specific conditions; the electrochemical risks specifically associated with HF signals must be investigated and established[102–106].

Finally, the HF amplitudes and net charge delivered per second can very quickly deplete implantable pulse generator (IPG) batteries, potentially necessitating more frequent surgical replacements, which have risks, or require use of a frequently rechargeable system[107].

HF signals are FDA-approved for abdominal vagus stimulation (aVNS) and peripheral nerve stimulation to treat obesity and post-amputation pain, respectively[47,108–113]. These therapies were predicated on the concept of blocking smaller diameter fibers that are responsible for sensations of hunger or pain. Rodent studies using LF to activate smaller diameter fibers and then HF to block the LF-evoked responses were used as evidence that HF could block smaller diameter fibers to support subsequent clinical efficacy studies. However, recent modeling and functional data have called into question whether HF at the levels often used clinically[47,110,111,114] are sufficient to block these smaller diameter fibers[48,49]. Critical determinants of the efficacy of HF such as the range of electrode-fiber distances, electrode size, and nerve anatomy are much different in rodents compared to humans or large animals[14,24]. Although it is hard to compare current levels across different electrode designs in different anatomical systems (abdominal and cervical VNs, peripheral nerves, etc.), our data indicates that the HF threshold to begin activating smaller diameter fibers is >10 mA in the ~3mm pig VN, and in turn, even higher amplitudes (≥20 mA) are required to block those fibers. Together with recent modeling studies, our data suggests that currently used clinical HF amplitudes are insufficient to block small diameter fibers[55]. Consequently, other mechanisms of action should be explored to explain the clinical effects, such as the consequence of HF-evoked asynchronous activation or influence of HF on pre- to post-synaptic fidelity at the synapse. These mechanisms are being investigated in another clinical application of HF, spinal cord stimulation (SCS) for pain, where the current delivered is set at sub-perception levels[115].

There are several additional limitations in this study that must be noted with an eye toward chronic application in human patients. First, experiments in this study were conducted in acute animals, under anesthesia, with an open surgical pocket with notably more exposure of the cervical vagus than would be present in a chronic implant. In particular, the average distance between the LF-VNS cuff and HF cuff was ~3.5 cm to prevent electric field interactions and enable disambiguation of their respective effects. In a human patient, this would require a large surgical pocket and placement of two separate cuffs; future work should be done to investigate how LF-VNS and HF effects interact when administered through a single cuff with relatively short distances between them. The anesthetized state also prevents the cuffs from moving relative to the anatomy as would normally occur from head and neck movements during daily activities. As previously mentioned, the distance between the HF electrode and fibers is critical in determining whether the effect of HF is blocking or asynchronously activating. Small movements between the cuff and underlying nerve could change the relationship between the HF electric field, the nerve, and any electrically excitable surrounding off-target structures. This would potentially lead to the transient phasing in and out of block effects or HF-induced activation of off-target side-effects. The open surgical pocket can also alter the distribution of electric fields and thus the associated block thresholds, both by any edema that occurs due to dissection, as well as air acting as insulation on the ventral side of the preparation; in our experiments all efforts were made to remove any buildup of edema (fluids) between stimulation trials. Acute responses may also differ from sustained chronic stimulation due to fibrous scarring/encapsulation of the electrodes, ongoing physiological activity, and potential habituation to LF and HF stimulation at the axonal, muscle, and central/synaptic levels.

Overall, the data presented in this study demonstrate that 10 kHz HF signals can block LF-VNS-evoked EMG and eCAP components—while conserving LF-VNS-evoked changes in HR—with previously unreported selectivity in a large animal model. These data demonstrate the feasibility of combining HF and LF signals to mitigate off-target activation of large diameter fibers during VNS that has adversely impacted several recent VNS clinical trials. Moreover, our results indicate that in the large animal model, HF activation and block exhibits the same order of stimulation recruitment as traditional LF stimulation, which has important implications for existing clinical HF therapies targeting small diameter fibers (e.g., SCS, aVNS). In summary, HF is a promising avenue for selective activation of small diameter fibers in neuromodulation, although much work remains to deploy HF as a reliable clinical solution, our data demonstrates HF's potential for increasing therapeutic current limits in applications limited by off-target large diameter fiber activation.

REFERENCES

1. Beekwilder, J. P. & Beems, T. Overview of the Clinical Applications of Vagus Nerve Stimulation. *J. Clin. Neurophysiol.* **27**, 130 (2010).
2. Koutsouras, D. A., Malliaras, G. G. & Langereis, G. The rise of bioelectronic medicine. *Bioelectron. Med.* **10**, 19 (2024).
3. Groves, D. A. & Brown, V. J. Vagal nerve stimulation: a review of its applications and potential mechanisms that mediate its clinical effects. *Neurosci. Biobehav. Rev.* **29**, 493–500 (2005).
4. Food and Drug Administration. Premarket Approval (PMA) P130019 MAESTRO RECHARGEABLE SYSTEM. *FDA Website* https://www.accessdata.fda.gov/scripts/cdrh/cfdocs/cfpma/pma.cfm?id=P130019.
5. Food and Drug Administration. Premarket Approval (PMA) P210007 Vivistim® System. *FDA Website* https://www.accessdata.fda.gov/scripts/cdrh/cfdocs/cfpma/pma.cfm?id=P210007.
6. Food and Drug Administration. Premarket Approval (PMA) P970003 VNS THERAPY SYSTEM. *FDA Website* https://www.accessdata.fda.gov/scripts/cdrh/cfdocs/cfpma/pma.cfm?id=P970003S050.
7. Food and Drug Administration. Premarket Approval (PMA) P970003 VNS THERAPY SYSTEM. *FDA Website* https://www.accessdata.fda.gov/scripts/cdrh/cfdocs/cfpma/pma.cfm?id=P970003.
8. SetPoint Medical Corporation. *Long Term Extension Study of the Safety and Efficacy of Neurostimulation Using a Vagus Nerve Stimulation Device in Patients With Rheumatoid Arthritis*. https://clinicaltrials.gov/study/NCT04862117 (2021).
9. Drewes, A. M. *Treatment of Complications to Diabetic Autonomic Neuropathy With Vagus Nerve Stimulation*. https://clinicaltrials.gov/study/NCT04143269 (2023).
10. Boston Scientific Corporation. *Neural Cardiac Therapy for Heart Failure Study*. https://clinicaltrials.gov/study/NCT01385176 (2024).
11. Câmara, R. & Griessenauer, C. J. Chapter 27 - Anatomy of the Vagus Nerve. in *Nerves and Nerve Injuries* (eds. Tubbs, R. S. et al.) 385–397 (Academic Press, San Diego, 2015). doi:10.1016/B978-0-12-410390-0.00028-7.
12. Pavlov, V. A. & Tracey, K. J. The vagus nerve and the inflammatory reflex—linking immunity and metabolism. *Nat. Rev. Endocrinol.* **8**, 743–754 (2012).

13. Hoffman, H. H. & Schnitzlein, H. N. The numbers of nerve fibers in the vagus nerve of man. *Anat. Rec.* **139**, 429–435 (1961).
14. Settell, M. L. *et al.* Functional vagotopy in the cervical vagus nerve of the domestic pig: implications for the study of vagus nerve stimulation. *J. Neural Eng.* **17**, 026022 (2020).
15. Nicolai, E. N. *et al.* Sources of off-target effects of vagus nerve stimulation using the helical clinical lead in domestic pigs. *J. Neural Eng.* **17**, 046017 (2020).
16. Blanz, S. L. *et al.* Spatially selective stimulation of the pig vagus nerve to modulate target effect versus side effect. *J. Neural Eng.* **20**, 016051 (2023).
17. Vuckovic, A., Tosato, M. & Struijk, J. J. A comparative study of three techniques for diameter selective fiber activation in the vagal nerve: anodal block, depolarizing prepulses and slowly rising pulses. *J. Neural Eng.* **5**, 275 (2008).
18. Musselman, E. D., Pelot, N. A. & Grill, W. M. Validated computational models predict vagus nerve stimulation thresholds in preclinical animals and humans. *J. Neural Eng.* **20**, 036032 (2023).
19. Yoo, P. B. *et al.* High-resolution measurement of electrically-evoked vagus nerve activity in the anesthetized dog. *J. Neural Eng.* **10**, 026003 (2013).
20. Fisher, B., DesMarteau, J. A., Koontz, E. H., Wilks, S. J. & Melamed, S. E. Responsive Vagus Nerve Stimulation for Drug Resistant Epilepsy: A Review of New Features and Practical Guidance for Advanced Practice Providers. *Front. Neurol.* **11**, 610379 (2020).
21. Handforth, A. *et al.* Vagus nerve stimulation therapy for partial-onset seizures. *Neurology* **51**, 48–55 (1998).
22. De Ferrari, G. M. *et al.* Long-term vagal stimulation for heart failure: Eighteen month results from the NEural Cardiac TherApy foR Heart Failure (NECTAR-HF) trial. *Int. J. Cardiol.* **244**, 229–234 (2017).
23. Chang, Y.-C. *et al.* Quantitative estimation of nerve fiber engagement by vagus nerve stimulation using physiological markers. *Brain Stimulat.* **13**, 1617–1630 (2020).
24. Pelot, N. A. *et al.* Quantified Morphology of the Cervical and Subdiaphragmatic Vagus Nerves of Human, Pig, and Rat. *Front. Neurosci.* **14**, 1148 (2020).
25. Musselman, E. D., Pelot, N. A. & Grill, W. M. Empirically Based Guidelines for Selecting Vagus Nerve Stimulation Parameters in Epilepsy and Heart Failure. *Cold Spring Harb. Perspect. Med.* **9**, a034264 (2019).

26. Ciotti, F. *et al*. Towards enhanced functionality of vagus neuroprostheses through in silico optimized stimulation. *Nat. Commun.* **15**, 6119 (2024).
27. Aristovich, K. *et al*. Model-based geometrical optimisation and *in vivo* validation of a spatially selective multielectrode cuff array for vagus nerve neuromodulation. *J. Neurosci. Methods* **352**, 109079 (2021).
28. Fitchett, A., Mastitskaya, S. & Aristovich, K. Selective Neuromodulation of the Vagus Nerve. *Front. Neurosci.* **15**, (2021).
29. Jayaprakash, N. *et al*. Organ- and function-specific anatomical organization of vagal fibers supports fascicular vagus nerve stimulation. *Brain Stimulat.* **16**, 484–506 (2023).
30. Ahmed, U. *et al*. Strategies for precision vagus neuromodulation. *Bioelectron. Med.* **8**, 9 (2022).
31. Ahmed, U. *et al*. Anodal block permits directional vagus nerve stimulation. *Sci. Rep.* **10**, 9221 (2020).
32. Wernisch, L. *et al*. Online Bayesian optimization of vagus nerve stimulation. *J. Neural Eng.* **21**, 026019 (2024).
33. Berthon, A. *et al*. Using neural biomarkers to personalize dosing of vagus nerve stimulation. *Bioelectron. Med.* **10**, 15 (2024).
34. Tosato, M., Yoshida, K., Toft, E. & Struijk, J. J. Quasi-trapezoidal pulses to selectively block the activation of intrinsic laryngeal muscles during vagal nerve stimulation. *J. Neural Eng.* **4**, 205 (2007).
35. Vuckovic, A., Tosato, M. & Struijk, J. J. A comparative study of three techniques for diameter selective fiber activation in the vagal nerve: anodal block, depolarizing prepulses and slowly rising pulses. *J. Neural Eng.* **5**, 275 (2008).
36. Austelle, C. W. *et al*. A Comprehensive Review of Vagus Nerve Stimulation for Depression. *Neuromodulation Technol. Neural Interface* **25**, 309–315 (2022).
37. Pérez-Carbonell, L., Faulkner, H., Higgins, S., Koutroumanidis, M. & Leschziner, G. Vagus nerve stimulation for drug-resistant epilepsy. *Pract. Neurol.* **20**, 189–198 (2020).
38. Thompson, N. *et al*. Organotopic organization of the porcine mid-cervical vagus nerve. *Front. Neurosci.* **17**, (2023).
39. Pečlin, P. & Rozman, J. Alternative Paradigm of Selective Vagus Nerve Stimulation Tested on an Isolated Porcine Vagus Nerve. *Sci. World J.* **2014**, 310283 (2014).

40. Thompson, N. *et al.* Fascicular Organisation and Neuroanatomy of the Porcine and Human Vagus Nerves: Allowing for Spatially Selective Vagus Nerve Stimulation. *FASEB J.* **36**, (2022).
41. Thompson, N. *et al.* Towards spatially selective efferent neuromodulation: anatomical and functional organization of cardiac fibres in the porcine cervical vagus nerve. *J. Physiol.* **n/a**,.
42. Chang, Y.-C. *et al.* kHz-frequency electrical stimulation selectively activates small, unmyelinated vagus afferents. *Brain Stimulat.* **15**, 1389–1404 (2022).
43. Nielsen, T. N., Struijk, J. J. & Sevcencu, C. Stimulation Waveforms for the Selective Activation of Baroreceptor Nerve Fibers in the Cervical Vagus Nerve. in *Converging Clinical and Engineering Research on Neurorehabilitation II* (eds. Ibáñez, J., González-Vargas, J., Azorín, J. M., Akay, M. & Pons, J. L.) 995–999 (Springer International Publishing, Cham, 2017). doi:10.1007/978-3-319-46669-9_161.
44. Muzquiz, M. I. *et al.* In-vivo application of low frequency alternating currents on porcine cervical vagus nerve evokes reversible nerve conduction block. *Bioelectron. Med.* **7**, 9 (2021).
45. Plachta, D. T. T. *et al.* Blood pressure control with selective vagal nerve stimulation and minimal side effects. *J. Neural Eng.* **11**, 036011 (2014).
46. Alhawwash, A. *et al.* In vivo peripheral nerve activation using sinusoidal low-frequency alternating currents. *Artif. Organs* **46**, 2055–2065 (2022).
47. Camilleri, M. *et al.* Intra-abdominal vagal blocking (VBLOC therapy): Clinical results with a new implantable medical device. *Surgery* **143**, 723–731 (2008).
48. Peña, E., Pelot, N. A. & Grill, W. M. Quantitative comparisons of block thresholds and onset responses for charge-balanced kilohertz frequency waveforms. *J. Neural Eng.* **17**, 046048 (2020).
49. Pelot, N. A. & Grill, W. M. In vivo quantification of excitation and kilohertz frequency block of the rat vagus nerve. *J. Neural Eng.* **17**, 026005 (2020).
50. Gerges, M. *et al.* Frequency- and amplitude-transitioned waveforms mitigate the onset response in high-frequency nerve block. *J. Neural Eng.* **7**, 066003 (2010).
51. Ackermann, D. M., Bhadra, N., Gerges, M. & Thomas, P. J. Dynamics and sensitivity analysis of high-frequency conduction block. *J. Neural Eng.* **8**, 065007 (2011).

52. Kilgore, K. L. & Bhadra, N. Nerve conduction block utilising high-frequency alternating current. *Med. Biol. Eng. Comput.* **42**, 394–406 (2004).

53. Peña, E., Pelot, N. A. & Grill, W. M. Non-monotonic kilohertz frequency neural block thresholds arise from amplitude- and frequency-dependent charge imbalance. *Sci. Rep.* **11**, 5077 (2021).

54. Peña, E., Pelot, N. A. & Grill, W. M. Spatiotemporal parameters for energy efficient kilohertz-frequency nerve block with low onset response. *J. NeuroEngineering Rehabil.* **20**, 72 (2023).

55. Pelot, N. A., Behrend, C. E. & Grill, W. M. Modeling the response of small myelinated axons in a compound nerve to kilohertz frequency signals. *J. Neural Eng.* **14**, 046022 (2017).

56. Avendaño-Coy, J., Serrano-Muñoz, D., Taylor, J., Goicoechea-García, C. & Gómez-Soriano, J. Peripheral Nerve Conduction Block by High-Frequency Alternating Currents: A Systematic Review. *IEEE Trans. Neural Syst. Rehabil. Eng.* **26**, 1131–1140 (2018).

57. Kapural, L. *et al.* Comparison of 10-kHz High-Frequency and Traditional Low-Frequency Spinal Cord Stimulation for the Treatment of Chronic Back and Leg Pain: 24-Month Results From a Multicenter, Randomized, Controlled Pivotal Trial. *Neurosurgery* **79**, 667 (2016).

58. Couto, J. & Grill, W. M. Kilohertz Frequency Deep Brain Stimulation Is Ineffective at Regularizing the Firing of Model Thalamic Neurons. *Front. Comput. Neurosci.* **10**, (2016).

59. Blanz, S. L. *et al.* Spatially selective stimulation of the pig vagus nerve to modulate target effect versus side effect. *J. Neural Eng.* **20**, 016051 (2023).

60. Verma, N. *et al.* Microneurography as a minimally invasive method to assess target engagement during neuromodulation. *J. Neural Eng.* **20**, 026036 (2023).

61. Deshmukh, A. *et al.* Epidural Spinal Cord Recordings (ESRs): sources of neural-appearing artifact in stimulation evoked compound action potentials. *J. Neural Eng.* (2024) doi:10.1088/1741-2552/ad7f8b.

62. Nicolai, E. N. *et al.* Vagus nerve stimulation using an endovascular electrode array. *J. Neural Eng.* **20**, 046008 (2023).

63. Gasser, H. S. & Erlanger, J. THE RÔLE PLAYED BY THE SIZES OF THE CONSTITUENT FIBERS OF A NERVE TRUNK IN DETERMINING THE FORM OF ITS ACTION POTENTIAL WAVE. *Am. J. Physiol.-Leg. Content* **80**, 522–547 (1927).

64. Woo, M. Y. & Campbell, B. ASYNCHRONOUS FIRING AND BLOCK OF PERIPHERAL NERVE CONDUCTION BY 20 KC ALTERNATING CURRENT. *Bull. Los Angel. Neurol. Soc.* **29**, 87–94 (1964).

65. ANTHEM-HFrEF Fails to Show Benefit of Vagal Nerve Stimulation Over GDMT. *TCTMD.com* https://www.tctmd.com/news/anthem-hfref-fails-show-benefit-vagal-nerve-stimulation-over-gdmt (2023).

66. School, M. M. Preliminary Findings from LivaNova's RECOVER Clinical Study on VNS Therapy for Treatment-Resistant Depression. *Louis A. Faillace, MD, Department of Psychiatry and Behavioral Sciences* https://med.uth.edu/psychiatry/2024/06/17/preliminary-findings-from-livanovas-recover-clinical-study-on-vns-therapy-for-treatment-resistant-depression/ (2024).

67. Pahuja, M. *et al.* Neuromodulation Therapies in Heart Failure: A State-of-the-Art Review. *J. Soc. Cardiovasc. Angiogr. Interv.* **2**, (2023).

68. Anand, I. S. *et al.* Comparison of symptomatic and functional responses to vagus nerve stimulation in ANTHEM-HF, INOVATE-HF, and NECTAR-HF. *ESC Heart Fail.* **7**, 75–83 (2020).

69. Ardell, J. L. *et al.* Defining the neural fulcrum for chronic vagus nerve stimulation: implications for integrated cardiac control. *J. Physiol.* **595**, 6887–6903 (2017).

70. Song, Z., Viisanen, H., Meyerson, B. A., Pertovaara, A. & Linderoth, B. Efficacy of Kilohertz-Frequency and Conventional Spinal Cord Stimulation in Rat Models of Different Pain Conditions. *Neuromodulation Technol. Neural Interface* **17**, 226–235 (2014).

71. Lee, K. Y. *et al.* Low-intensity, Kilohertz Frequency Spinal Cord Stimulation Differently Affects Excitatory and Inhibitory Neurons in the Rodent Superficial Dorsal Horn. *Neuroscience* **428**, 132–139 (2020).

72. Dai, F., Yin, J. & Chen, J. D. Z. Effects and Mechanisms of Vagal Nerve Stimulation on Body Weight in Diet-Induced Obese Rats. *Obes. Surg.* **30**, 948–956 (2020).

73. Wang, D., Lee, K. Y., Lee, D., Kagan, Z. B. & Bradley, K. Low-Intensity 10 kHz Spinal Cord Stimulation Reduces Behavioral and Neural Hypersensitivity in a Rat Model of Painful Diabetic Neuropathy. *J. Pain Res.* **15**, 1503–1513 (2022).

74. Bender, S. A. *et al.* Closed-Loop Multimodal Neuromodulation of Vagus Nerve for Control of Heart Rate*. in *2024 American Control Conference (ACC)* 4536–4541 (2024). doi:10.23919/ACC60939.2024.10644421.

75. Ackermann Jr., D. M. *et al.* Electrical conduction block in large nerves: High-frequency current delivery in the nonhuman primate. *Muscle Nerve* **43**, 897–899 (2011).

76. Knutson, J. S. *et al.* First-in-Human Demonstration of High-Frequency Electrical Motor Nerve Block: Case Report. *Am. J. Phys. Med. Rehabil.* **104**, e37 (2025).

77. Fjordbakk, C. T. *et al.* Feasibility of kilohertz frequency alternating current neuromodulation of carotid sinus nerve activity in the pig. *Sci. Rep.* **9**, 18136 (2019).

78. Fisher, K. M., Jillani, N. E., Oluoch, G. O. & Baker, S. N. Blocking central pathways in the primate motor system using high-frequency sinusoidal current. *J. Neurophysiol.* **113**, 1670–1680 (2015).

79. Kilgore, K. L. & Bhadra, N. Reversible Nerve Conduction Block Using Kilohertz Frequency Alternating Current. *Neuromodulation J. Int. Neuromodulation Soc.* **17**, 242–255 (2014).

80. Bhadra, N., Foldes, E., Vrabec, T., Kilgore, K. & Bhadra, N. Temporary persistence of conduction block after prolonged kilohertz frequency alternating current on rat sciatic nerve. *J. Neural Eng.* **15**, 016012 (2018).

81. Bhadra, N., Lahowetz, E. A., Foldes, S. T. & Kilgore, K. L. Simulation of high-frequency sinusoidal electrical block of mammalian myelinated axons. *J. Comput. Neurosci.* **22**, 313–326 (2007).

82. Hernandez, C. M. & Richards, J. R. Physiology, Sodium Channels. in *StatPearls* (StatPearls Publishing, Treasure Island (FL), 2024).

83. Miles, J. D., Kilgore, K. L., Bhadra, N. & Lahowetz, E. A. Effects of ramped amplitude waveforms on the onset response of high-frequency mammalian nerve block. *J. Neural Eng.* **4**, 390 (2007).

84. Rosenblueth, A. & Reboul, J. THE BLOCKING AND DEBLOCKING EFFECTS OF ALTERNATING CURRENTS ON NERVE. *Am. J. Physiol.-Leg. Content* **125**, 251–264 (1939).

85. Vargas, L., Musselman, E. D., Grill, W. M. & Hu, X. Asynchronous axonal firing patterns evoked via continuous subthreshold kilohertz stimulation. *J. Neural Eng.* **20**, 026015 (2023).

86. Franke, M. *et al.* Combined KHFAC + DC nerve block without onset or reduced nerve conductivity after block. *J. Neural Eng.* **11**, 056012 (2014).

87. Patel, Y. A. & Butera, R. J. Challenges associated with nerve conduction block using kilohertz electrical stimulation. *J. Neural Eng.* **15**, 031002 (2018).

88. Yi, G. & Grill, W. M. Kilohertz waveforms optimized to produce closed-state Na+ channel inactivation eliminate onset response in nerve conduction block. *PLOS Comput. Biol.* **16**, e1007766 (2020).

89. Ackermann, D. M., Bhadra, N., Foldes, E. L. & Kilgore, K. L. Conduction block of whole nerve without onset firing using combined high frequency and direct current. *Med. Biol. Eng. Comput.* **49**, 241–251 (2011).

90. Okonogi, T. *et al.* Stress-induced vagal activity influences anxiety-relevant prefrontal and amygdala neuronal oscillations in male mice. *Nat. Commun.* **15**, 183 (2024).

91. Conway, C. R. & Xiong, W. The Mechanism of Action of Vagus Nerve Stimulation in Treatment-Resistant Depression: Current Conceptualizations. *Psychiatr. Clin. North Am.* **41**, 395–407 (2018).

92. Lai, J. & David, S. V. Short-Term Effects of Vagus Nerve Stimulation on Learning and Evoked Activity in Auditory Cortex. *eNeuro* **8**, (2021).

93. Loerwald, K. W., Borland, M. S., Rennaker, R. L., Hays, S. A. & Kilgard, M. P. The interaction of pulse width and current intensity on the extent of cortical plasticity evoked by vagus nerve stimulation. *Brain Stimulat.* **11**, 271–277 (2018).

94. Borland, M. S. *et al.* Cortical Map Plasticity as a Function of Vagus Nerve Stimulation Intensity. *Brain Stimulat.* **9**, 117–123 (2016).

95. The pathophysiology of spasticity - Sheean - 2002 - European Journal of Neurology - Wiley Online Library. https://onlinelibrary.wiley.com/doi/full/10.1046/j.1468-1331.2002.0090s1003.x.

96. Marom, S. & Marder, E. A biophysical perspective on the resilience of neuronal excitability across timescales. *Nat. Rev. Neurosci.* **24**, 640–652 (2023).

97. Persson, A.-K., Hoeijmakers, J. G. J., Estacion, M., Black, J. A. & Waxman, S. G. Sodium Channels, Mitochondria, and Axonal Degeneration in Peripheral Neuropathy. *Trends Mol. Med.* **22**, 377–390 (2016).

98. Taylor, A. L., Goaillard, J.-M. & Marder, E. How Multiple Conductances Determine Electrophysiological Properties in a Multicompartment Model. *J. Neurosci.* **29**, 5573–5586 (2009).

99. Rosario, J. S. D. *et al.* Sustained Depolarization Induces Homeostatic Plasticity in Mouse and Human Sensory Neurons. *J. Pain* **23**, 6 (2022).

100. Franke, M., Bhadra, N., Bhadra, N. & Kilgore, K. Direct current contamination of kilohertz frequency alternating current waveforms. *J. Neurosci. Methods* **232**, 74–83 (2014).

101. Shannon, R. V. A model of safe levels for electrical stimulation. *IEEE Trans. Biomed. Eng.* **39**, 424–426 (1992).
102. Cogan, S. F., Ludwig, K. A., Welle, C. G. & Takmakov, P. Tissue damage thresholds during therapeutic electrical stimulation. *J. Neural Eng.* **13**, 021001 (2016).
103. Shannon, R. V. A model of safe levels for electrical stimulation. *IEEE Trans. Biomed. Eng.* **39**, 424–426 (1992).
104. Cogan, S. F., Hara, S. & Ludwig, K. A. Chapter 7 - The Safe Delivery of Electrical Currents and Neuromodulation. in *Neuromodulation (Second Edition)* (eds. Krames, E. S., Peckham, P. H. & Rezai, A. R.) 83–94 (Academic Press, 2018). doi:10.1016/B978-0-12-805353-9.00007-3.
105. Wilks, S. J. *et al.* Non-clinical and Pre-clinical Testing to Demonstrate Safety of the Barostim Neo Electrode for Activation of Carotid Baroreceptors in Chronic Human Implants. *Front. Neurosci.* **11**, (2017).
106. Li, Y. *et al.* NeurostimML: A machine learning model for predicting neurostimulation-induced tissue damage. *bioRxiv* 2023.10.18.562980 (2023) doi:10.1101/2023.10.18.562980.
107. Ikramuddin, S. *et al.* Effect of reversible intermittent intra-abdominal vagal nerve blockade on morbid obesity: the ReCharge randomized clinical trial. *JAMA* **312**, 915–922 (2014).
108. Johannessen, H. *et al.* Vagal Blocking for Obesity Control: a Possible Mechanism-Of-Action. *Obes. Surg.* **27**, 177–185 (2017).
109. Finch, P., Price, L. & Drummond, P. High-Frequency (10 kHz) Electrical Stimulation of Peripheral Nerves for Treating Chronic Pain: A Double-Blind Trial of Presence vs Absence of Stimulation. *Neuromodulation Technol. Neural Interface* **22**, 529–536 (2019).
110. Apovian, C. M. *et al.* Two-Year Outcomes of Vagal Nerve Blocking (vBloc) for the Treatment of Obesity in the ReCharge Trial. *Obes. Surg.* **27**, 169–176 (2017).
111. Shikora, S. A. *et al.* Sustained Weight Loss with Vagal Nerve Blockade but Not with Sham: 18-Month Results of the ReCharge Trial. *J. Obes.* **2015**, 365604 (2015).
112. Khalid, S. I., Veludandi ,Nikhil, Agwu ,Chibueze & and Slavin, K. V. Altius electrical nerve stimulation for post-amputation pain treatment: a comprehensive review. *Pain Manag.* **0**, 1–7.

113. Kapural, L. *et al.* Long-Term Treatment of Chronic Postamputation Pain With Bioelectric Nerve Block: Twelve-Month Results of the Randomized, Double-Blinded, Cross-Over QUEST Study. *Neuromodulation Technol. Neural Interface* **27**, 1383–1392 (2024).
114. Waataja, J. J., Tweden, K. S. & Honda, C. N. Effects of high-frequency alternating current on axonal conduction through the vagus nerve. *J. Neural Eng.* **8**, 056013 (2011).
115. Rogers, E. R., Mirzakhalili, E. & Lempka, S. F. Model-based analysis of subthreshold mechanisms of spinal cord stimulation for pain. *J. Neural Eng.* **20**, 066003 (2023).

FIGURES

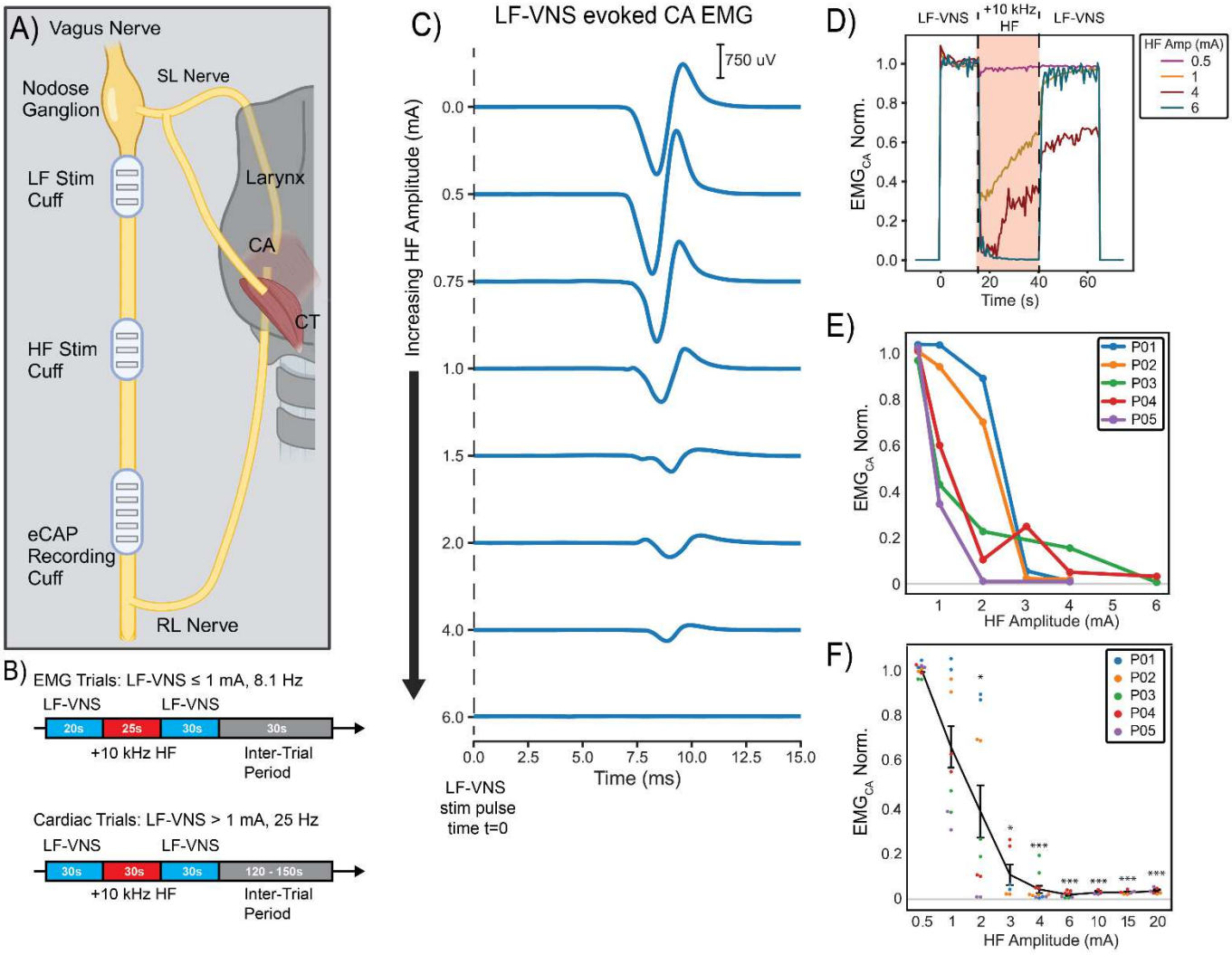


Figure 1: 10 kHz HF blocks LF-VNS-evoked muscle activity. **A)** Schematic of experimental preparation in anesthetized pigs. Low-frequency vagus nerve stimulation (LF-VNS) was delivered ~1 cm caudal to the nodose ganglion, high-frequency (HF) signals were applied ~3.5 cm caudal to the LF-VNS cuff, and evoked compound action potentials (eCAPs) were recorded ~6.25 cm caudal to __. Muscle activity was recorded from the cricoarytenoid (CA) muscle with bipolar EMG electrodes (EMG_{CA}). **B)** Schematic of LF-VNS + HF trials subdivided into EMG- and cardiac-focused trials, due to the higher signal amplitudes and longer trial durations required to study cardiac effects. **C)** Example stimulus-triggered averages of the LF-VNS-evoked muscle activity (EMG_{CA}) during the HF-period at increasing amplitudes of 10 kHz HF (subject P03). To quantify this effect, we calculated the area-under-the-curve (AUC (V_{rms})) of the EMG_{CA} response during the LF-VNS trial. **D)** LF-VNS-evoked EMG_{CA} over four stimulation trials at different HF amplitudes (subject P03). Data were normalized within trial against the pre-HF (LF-VNS only) period. **E)** Dose-response curves of LF-VNS evoked EMG_{CA} from all subjects. **F)** Cohort averaged dose-response curve of LF-VNS evoked muscle activity (EMG_{CA}) at all HF amplitudes. Data are from combined EMG-focused (HF < 6 mA) and cardiac-focused (HF > 6 mA) trials with larger HF step-sizes (i.e. x-axis is non-linear). Dots represent individual subjects, solid line and error bars denote mean ± 1 standard error. Aggregated data were tested using the non-parametric Kruskal-Wallis test (Kruskal H = 49.22, $p < 0.001$) followed by Dunn's test post-hoc comparison against 0.5 mA HF with Holm-Sidak correction for multiple comparisons. * $p < 0.05$, *** $p < 0.001$.

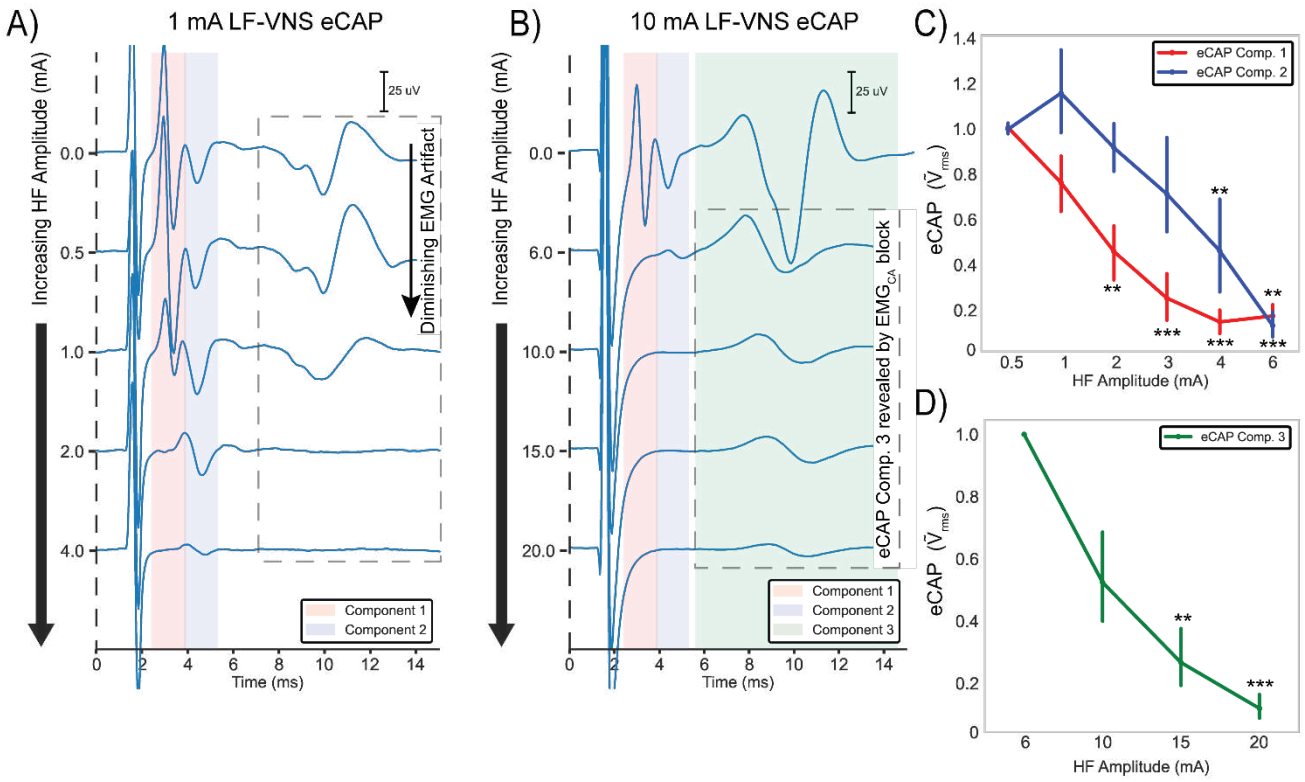
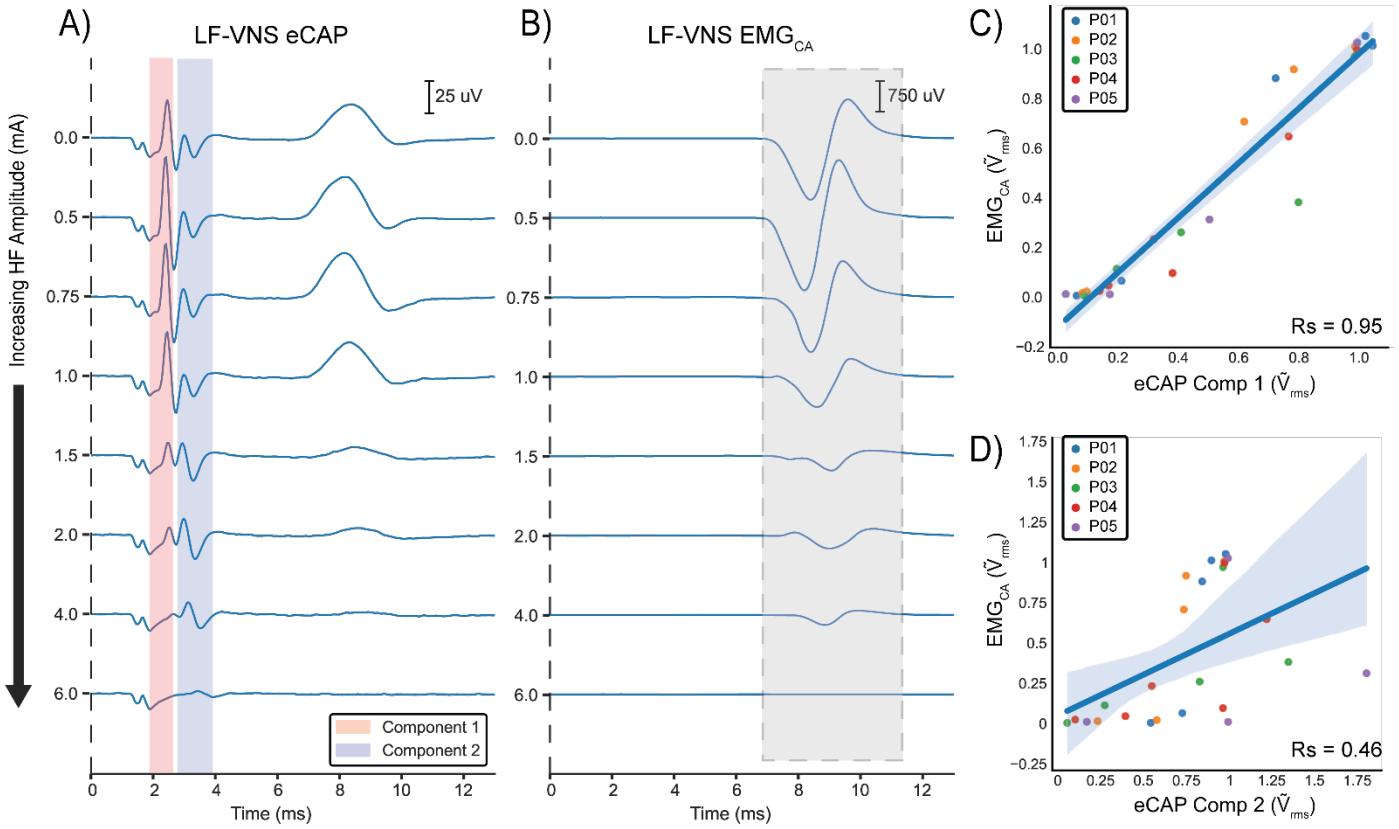


Figure 2: Components of the LF-VNS-evoked nerve response (eCAP) are selectively blocked by increasing amplitudes of 10 kHz HF. A, B) Example stimulus-triggered average of the evoked compound action potential (eCAP) elicited by 1 mA (A) or 10 mA (B) low-frequency vagus nerve stimulation (LF-VNS, 8.1 Hz in 1 mA trial, 25 Hz in 10 mA trial) during the high-frequency (HF) period, with increasing HF amplitudes (subject P05, see Supplemental Figure 4 for all subjects). The 0 mA HF response is the averaged pre-HF eCAP from all trials. **C, D)** Normalized ($\tilde{V}_{rms}$) of the eCAP components across HF amplitudes. Data were normalized within trial against the pre-HF (LF-VNS only) period. Error bars = ± 1 standard error of the mean. Aggregated data were analyzed via the same methods as EMG_{CA} (Component 1 Kruskal H = 39.22 $p < 0.001$, Component 2 Kruskal H = 28.55 $p < 0.001$, Component 3 Kruskal H = 19.49, $p < 0.001$; * $p < 0.05$, ** $p < 0.01$, ***$p < 0.001$ Dunn's post-hoc Holm-Sidak corrected p). Subjects (P01, P04) who exhibited short-latency, superior laryngeal-mediated EMG responses were excluded from Component 3 analysis.

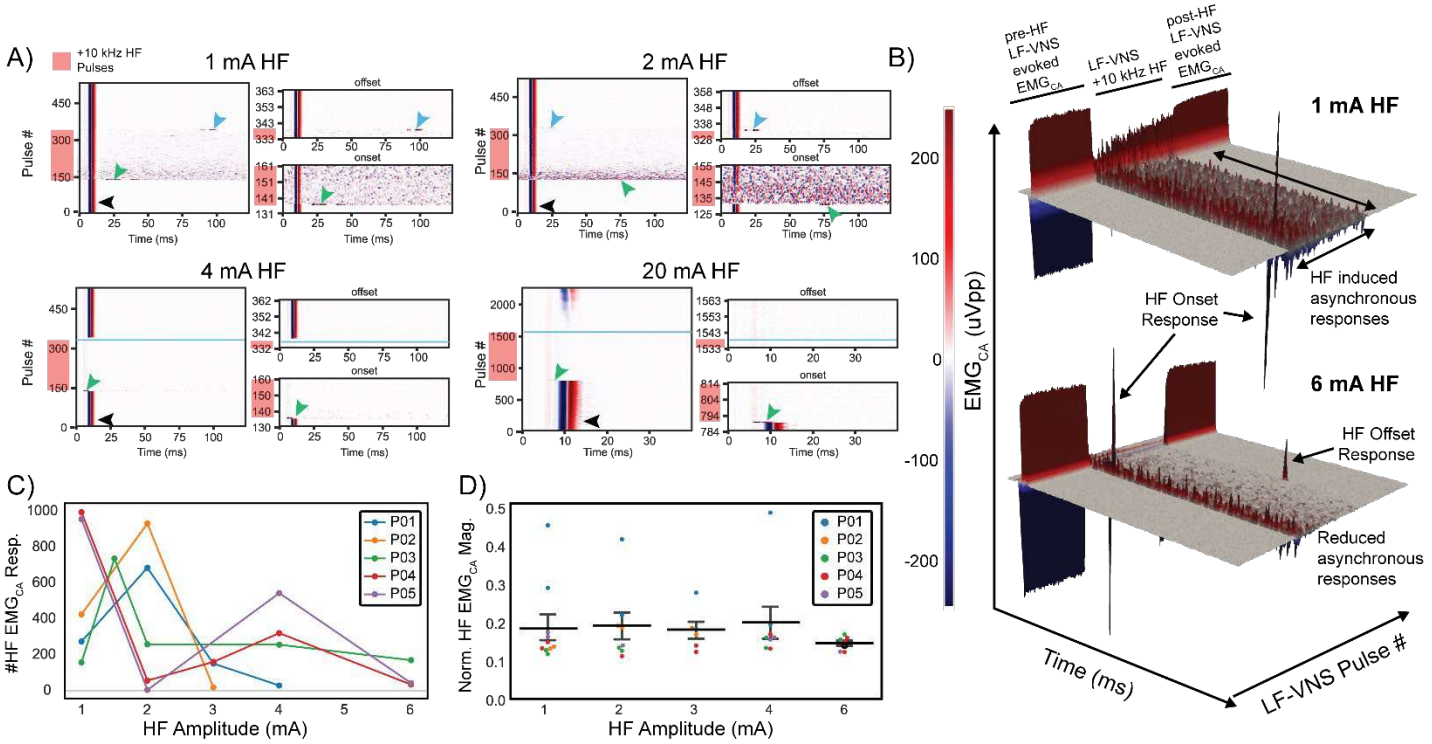


652

653 **Figure 3**: **Short-latency component of the LF-VNS-evoked eCAP correlated with the evoked EMG$_{CA}$. A,**
654 **B)** Example (subject P03) paired eCAP and EMG$_{CA}$ responses to 1 mA LF-VNS at successively increasing HF
655 amplitudes. As the HF amplitude is increased, the block (reduced magnitude) of the first component of the
656 eCAP (red-shaded region) tracks the reduced magnitude of the evoked EMG$_{CA}$ (gray-shaded region). **C, D)**
657 Correlation between the evoked EMG$_{CA}$ against the first (C) and second (D) eCAP components. The eCAP
658 component and EMG$_{CA}$ were normalized ($\tilde{V}_{rms}$) within trial against their respective pre-HF (LF-VNS only)
659 signals. Dots represent individual subjects, solid lines denote the linear regression, and shaded regions denote
660 95% confidence interval. Rs = Spearman's correlation coefficient.

661

662 $\tilde{V}_{rms}$



663

664 **Figure 4: Onset features of the HF response scaled with HF amplitude. A)** Rasterized plots of the EMG_{CA}
665 response to LF-VNS (1 mA, 8.1 Hz in 1-4 mA HF trials, 25 Hz in 20 mA HF trial) and increasing HF amplitude
666 (subject P05). The x axes are time, with t=0 corresponding to the initiation of a single LF-VNS stimulation pulse.
667 The y axes denote the LF-VNS pulse number for a given trial with pulses during HF shaded in red. Color
668 represents the magnitude of the EMG_{CA} signal. The LF-VNS-evoked EMG_{CA} is seen in the darkly colored (high
669 amplitude) vertical bars towards the left of each plot (black arrowheads), shortly after the LF-VNS stimulation
670 pulse at t=0. Corresponding sub-panels show zooms of the periods before the initiation (5 LF-VNS pulses) and
671 after the termination (25 LF-VNS pulses) of the 10 kHz HF signal. Initiation of HF (green arrowheads) was
672 always accompanied by a single, rapid onset response. Complete block of the LF-VNS-evoked EMG_{CA} is
673 evidenced by the absence of darkly colored bars during HF at higher amplitudes (4 and 20 mA) whereas sub-
674 block HF amplitudes (1 and 2 mA) had no appreciable effect on LF-VNS responses. Offset of HF is denoted by
675 the blue arrowheads/lines with arrowheads used in trials where an offset EMG_{CA} response was observed and
676 lines when no offset response was present. **B)** Three-dimensional representation of rasterized EMG_{CA} plots.
677 **C)** Quantification of the number of asynchronous muscle responses during the HF period as a function of HF
678 amplitude. Peaks with an amplitude >10% of the LF-VNS-evoked EMG_{CA} were counted as asynchronous
679 responses. HF amplitudes for which no asynchronous responses were detected are not plotted (e.g., P02 >3
680 mA HF). **D)** The magnitude of HF-evoked asynchronous responses were not dependent on the HF amplitude
681 and consistently ~20% of the amplitude of the EMG_{CA} evoked by 1 mA LF-VNS. Data were normalized against
682 the pre-HF LF-VNS-evoked EMG_{CA}; Kruskal-H = 2.59, p = 0.62.

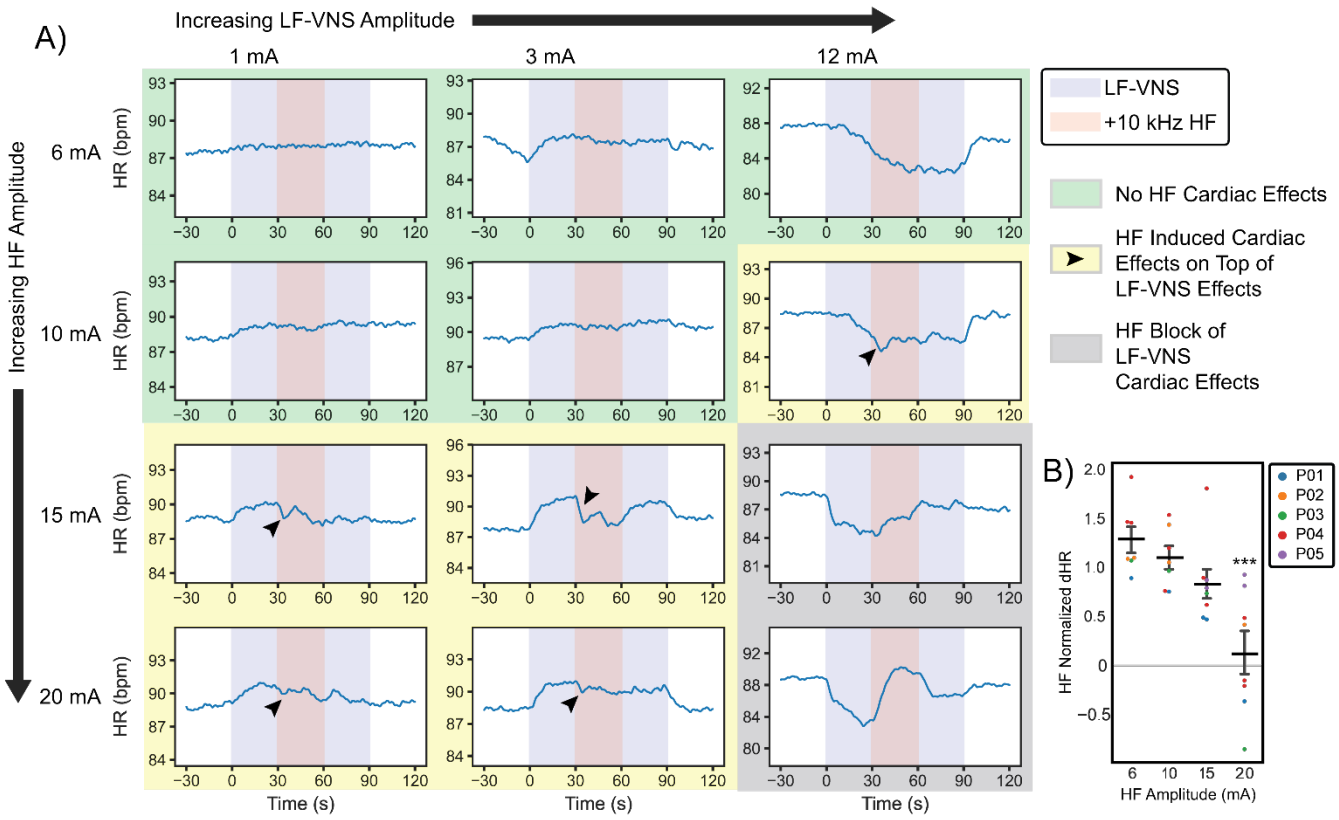


Figure 5: HF blocking signal effects on LF-VNS evoked cardiac response. A) Heart rate from a representative animal (subject P05) in response to increasing amplitudes of LF-VNS (25 Hz in all trials) and HF. Panels with a green background denote trials in which there were no HF-induced cardiac effects observed. Panels with a yellow background denote trials in which the onset of HF induced some cardiac effect. Panels with a gray background denote trials where the HF blocked the LF-VNS evoked bradycardia. **B)** Effect of HF on LF-VNS cardiac effects. HR from trials in which bradycardia was evoked were binned based on HF amplitude and the change in HR (dHR) during HF was normalized by the pre-HF dHR (see Methods Eq. 2). A value of 1 indicates no difference between the maximum HR difference from baseline between the 'pre-HF, LF-VNS only' (1st blue-shaded region) and '+10 kHz HF' (red-shaded region) periods whereas a value close to 0 indicates that the maximum HR difference during HF returned to near baseline. Negative values indicate that the HR during the HF period was above baseline (tachycardia) during the last 10 s of HF. Kruskal-Wallis H = 15.97, p = 0.001, Dunn's post-hoc vs. 6 mA HF with Holm-Sidak correction *** p < 0.001

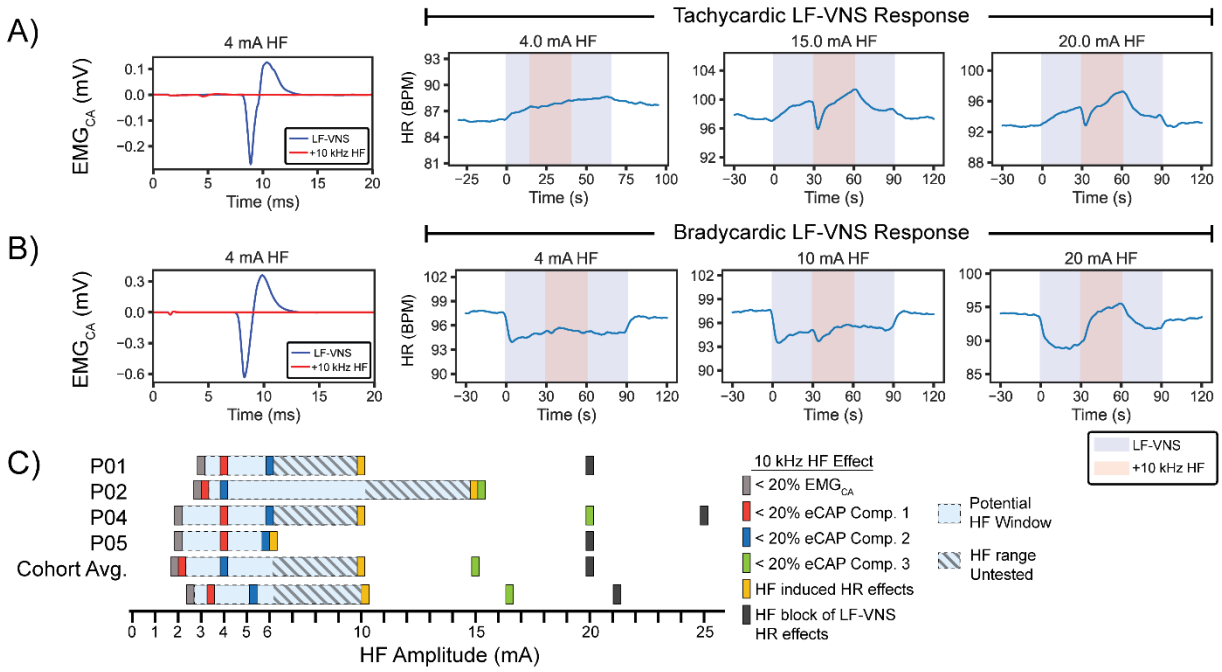
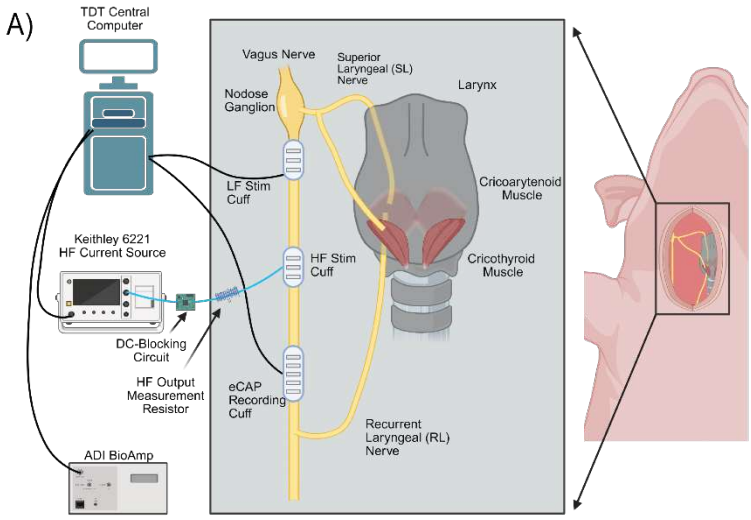


Figure 6: HF can completely block LF-VNS-evoked EMG$_{CA}$ without influencing LF-VNS-evoked heart rate changes. A) Paired EMG$_{CA}$ and HR recordings from a representative subject (P02) with LF-VNS amplitude titrated to elicit a tachycardic response (LF-VNS 25 Hz, 1 mA during 4 mA HF trial and 3 mA during 15/20 mA HF trials). At these LF-VNS/HF amplitudes, the EMG$_{CA}$ was completely blocked (left plot, red trace) with no HF-induced cardiac effects observed until 15 mA. **B)** The same observation when the LF-VNS amplitude was set to induce bradycardia (LF-VNS 25 Hz, 8 mA for all trials). **C)** Colored bars indicate the HF amplitudes for each response type. The bar was placed at the lowest HF amplitude for which each effect was seen across all trials from that subject. Bottom row represents the cohort mean HF amplitude for each effect; across the cohort, there was an HF amplitude range wherein the 10 kHz HF blocked the LF-VNS evoked EMG$_{CA}$ without any HF-induced cardiac effects ('HF window', light blue shaded region). Note that not all HF amplitudes across this range were tested in our trials; the HF amplitudes tested are denoted by numeric value on the x-axis. Therefore, the HF window may be smaller than shown here as lower HF amplitudes within the untested range (striped region) may evoke brief, asynchronous activation of small diameter cardiac efferents and subsequent HR effects.

METHODS

All experiments were approved by the University of Wisconsin-Madison Institutional Animal Care and Use Committee (IACUC). The experimental cohort consisted of n = 5 domestic (Yorkshire/Landrace) swine (3 female / 2 males, mean weight = 49.02 ± 4.52 kg) housed with *ad libitum* access to water, fed twice daily, and under a 12-hour light/dark cycle. On the day of the experiment, subjects were induced with a combination of telazol (6 mg/kg) and xylazine (2 mg/kg) before being intubated, mechanically ventilated, and moved to isoflurane (1.5-2 %) and fentanyl (5-12 μg/kg/hr) anesthesia for the remainder of the experiment. Heart rate (HR), blood oxygenation (SpO_2), expiratory capnograph (CO_2), blood pressure (BP), and temperature were continuously monitored using a veterinary surgical monitor (BioNet BM5Vet Elite, Seoul, South Korea) in all subjects to monitor depth of anesthesia. Separately, electrocardiogram (ECG) and strain-gauge pulse transducer time series were also collected using an ADInstruments PowerLab 8/35 system (sampling rate 1 kHz, Sydney, Australia) and LabChart 8 software configured to provide real-time calculation of HR and synchronize with our electrophysiological stimulation and recording system. In a subset of subjects (n = 3/5), arterial blood pressure (aBP) was also collected using a Millar catheter (Millar Inc., Houston, TX, Model #SPR-350S) introduced via the femoral artery and recorded by ADInstruments/LabChart. All experiments were performed on the right cervical vagus nerve (VN) which was surgically isolated from surrounding tissue from the nodose ganglion to the sternal notch. In the first subject (subject P01), the sympathetic trunk was traveling with the VN and was not separately isolated, leading to strong stimulation-evoked tachycardia. Thus, for all remaining subjects, extra care was taken to identify and isolate the vagus and sympathetic trunk from each other when they were found conjoined.

In each experiment, nerve cuffs were placed along the length of the VN as follows (Methods Figure 1A). First, a custom multi-contact circumferential cuff (inner diameter (I.D.) 3mm, contact spacing 3mm center-to-center, inner contacts = 2mm square, outer contacts = 1mm strip) was placed ~ 0.7–1 cm caudal to the nodose ganglion for application of low-frequency vagus nerve stimulation (LF-VNS). Next, a multi-channel longitudinal full-wrap cuff (5-channel, I.D. 3 mm, contact spacing 2 mm center-to-center, all contacts = 1 mm strip, Ardiem Medical, Indiana PA, USA) was placed on the vagus further along the VN at the most caudal end of the surgical window to collect evoked compound action potential (eCAP) recordings. Finally, a 3-channel longitudinal full-wrap cuff (same dimensions as eCAP cuff minus two channels, Ardiem Medical, Indiana PA, USA) for application of the HF signal was placed approximately equidistant between the LF-VNS stimulation and eCAP recording cuffs. As the size of the surgical window varied across subjects, this approach of relative cuff positioning maximizing the distance between cuffs was taken to achieve the greatest separation between cuffs and minimize interactions between them (see Methods Figure 1C). To measure evoked muscle activity, bipolar electromyography (EMG) leads (RLSND121-2.5; RhythmLink, Columbia SC, USA) were placed into both the cricoarytenoid (CA) and cricothyroid (CT) muscles.



C)

Cuff Distances		
Subject	LF-VNS to HF (mm)	LF-VNS to eCAP recording (mm)
P01	32	75
P02	35	67
P03	31	62
P04	37	60
P05	38	77
Cohort Mean (mm)	34.6	68.2
Standard Error (mm)	1.36381817	3.39705755

Methods Figure 1: Experimental Preparation. A) Surgical/instrumentation diagram. B) Schematic of LF-VNS/HF trials. C) Table of relative cuff distances across subjects.

Hardware and Instrumentation

The LF-VNS stimulation cuff, eCAP recording cuff, and EMG leads were connected to the respective stimulation and recording banks of a Tucker-Davis Technologies (TDT) 64-channel electrophysiology system (sampling rate, f_s = 24414 Hz, RZ2, IZV10, SI8, WS8; TDT, Alachua FL, USA), which was controlled using TDT's Synapse Software. The muti-channel circumferential LF-VNS stimulation cuff was set-up in a tripolar configuration (center channel cathode). eCAP recording channels were single-channel recordings referenced against a needle placed into the fat layer at the superficial aspects of the pocket at approximately the same cranial-caudal plane as the eCAP cuff. EMG was recorded in differential mode across the two leads of the bipolar EMG electrodes. Stainless steel pads were placed beneath the animal to serve as stimulation and recording grounds. Synapse/TDT was configured to output a TTL-pulse to a dedicated channel on the ADInstruments PowerLab 8/35 to synchronize stimulation events with physiologic measures.

The HF cuff was also configured for tripolar stimulation (center channel cathode) to limit the amount of HF artifact present. The instrumentation for delivering and quantifying the HF waveform varied slightly across subjects (Supplemental Figure 9) as we developed the experimental preparation. In summary, a Keithley current source (Keithley 6221; Tektronix, Beaverton OR, USA) controlled via network connection by a custom Python script was used to specify the parameters of the HF waveform. Based on previous studies, we were initially concerned that the output of the Keithley 6221 may be attenuated due to the combination of large load (electrode impedance), high frequency (10 kHz), and high current amplitudes. As a result, in some experiments (n = 2/5), an AM-Systems 4100 linear stimulus isolator was used as a pass-through amplifier for the Keithley's output as in Pelot and Grill 2020[1]. However, upon further investigation, we found that our electrodes, which are larger in size than electrodes used in rodent studies, had sufficiently low impedance to avoid significant attenuation of the Keithley 6221 output at 10 kHz. Further, we found that the AM-Systems 4100 could introduce significant noise in eCAP recordings; therefore, the rest of the experiments (n = 3/5) were performed without the AM-Systems 4100 in the circuit. Regardless of the current source, a DC-blocking circuit[2,3] comprised of 1 µF capacitors and 100 kΩ resistors was placed in series with the HF output to prevent build-up of DC offset during HF stimulation. In addition, a 100 Ω resistor was placed into the HF circuit to assess the actual HF current delivered (measured via TDT's built-in ADC (P01,P02) or a Keithley 6510 (P03-P05) in each subject accounting for differences in electrode impedance across subjects (Supplemental Figure 9).

Experimental Protocol

Experimental trials were broadly divided into 'EMG' and 'Cardiac' trial sets wherein the goal of each category was to characterize the effect of HF on the LF-VNS-evoked muscle and HR responses, respectively. In all cases, the frequency of HF was 10 kHz, and the LF-VNS consisted of 250 µs/phase symmetric biphasic

pulses. An individual trial set consisted of multiple LF-VNS amplitudes (randomized order) with a specific HF amplitude. Within each individual trial the presentation of LF-VNS and HF were configured to begin with an initial LF-VNS only period to establish the effects of LF-VNS followed by a combined LF-VNS + HF period to assess the effect of HF on the LF-VNS response, and lastly a post-HF LF-VNS period to assess the recovery of the LF-VNS response after HF (Methods Figure 1B).

EMG and Cardiac trials differed in the following ways; first, the frequency of LF-VNS in the Cardiac trials was set at 25 Hz consistent with current clinical investigations of LF-VNS for heart failure while the frequency in the EMG trials was set to 8.1 Hz. The lower frequency of the EMG trials was to prevent diminishment of the EMG signal due to muscle fatigue being mistaken as block of motor fiber conduction. Second, the duration of trial phases (i.e. pre-HF, during-HF, post-HF, and inter-stimulation periods) were longer in the Cardiac than EMG trials to account for the slower heart rate responses (both during stimulation and recovery after stimulation Methods Figure 1B). Lastly, the range of LF-VNS and HF amplitudes applied in the EMG and Cardiac trials differed with both LF-VNS and HF amplitudes being smaller in EMG trials (LF-VNS ≤1 mA, HF ≤6 mA) than those applied in Cardiac trials (LF-VNS up to 12 mA, HF up to 25 mA).

The LF-VNS amplitude was limited during EMG trials to avoid causing longer duration cardiac effects which would have required a longer inter-stimulation period to washout. Based on our previous studies in pigs, a LF-VNS current amplitude of 1 mA is sufficient to reliably evoke large EMG responses while avoiding significant cardiac effects[4]. In contrast, due to intersubject variability, the LF-VNS amplitude range during Cardiac trials was empirically determined by incrementally increasing the LF-VNS amplitude until a sustained bradycardic response was evoked. Likewise, HF amplitudes were empirically determined *ad hoc* by incrementally increasing the HF amplitude in a separate thresholding process where the LF-VNS amplitude was maintained at a constant level which evoked either strong visual neck muscle contractions (EMG trials, LF-VNS = 1 mA) or sustained bradycardia (Cardiac trials, LF-VNS varied by subect). The HF range was then determined by incrementally increasing the HF amplitude applied until A) application of HF caused visual cessation of the LF-VNS evoked neck muscle activation (EMG trials) or B) application of HF caused a reversal of the LF-VNS evoked bradycardia (Cardiac trials). For experimental comparison, we maintained relatively constant HF amplitudes within the EMG trials; however, the number of HF amplitudes tested within the Cardiac trials varied across subjects due to the substantially longer Cardiac trial times and experimental time constraints of our protocol (12-hrs from induction).

We previously showed that the electrical field generated by evoked muscle activity can contaminate neural eCAP recordings from the VN—i.e., EMG artifact—in such a way as to cause potential misinterpretation of the eCAP[4,5]. Within the context of cervical VNS, activation of the CA and CT muscles may appear as components in the eCAP signal with a latency of approximately 5 – 10 ms post-stimulus which, depending on the distance between cuffs, places their conduction velocity in the slow Aδ to B-fiber range[6]. In many of our trials, application of HF signal removed this contamination by preventing activation of the CA/CT muscles via conduction block (Figure 2). However, to confirm all eCAP components analyzed were neural in origin, we also performed a set of experimental trials with a muscle paralytic (vecuronium bromide, 1 mg/kg/hr) in a subset (n = 3/5) of subjects (Supplemental Figure 3).

Data Analysis

To remove the 10 kHz HF artifact from the eCAP and EMG recordings, we used a custom software package developed by our lab for handling electrophysiological datasets (pyeCAP: https://github.com/ludwig-lab/pyeCAP). We used a multi-step filtering process consisting of a 1D Gaussian low-pass filter (sigma = 1.29) to remove the majority of the HF artifact followed by a notch filter centered at 10 kHz to further attenuate any residual 10 kHz signal, and lastly a median high-pass filter (kernel = 201) to address any baseline drift (Supplemental Figures 10, 11).

Identification of HF Start and End: Although the HF output was controlled via the TDT system's computer, there was no direct synchronization between the Synapse software controlling the LF-VNS stimulation train and the Python script controlling HF output. To identify the specific LF-VNS pulses corresponding to the HF start and end times, we developed a simple algorithm which was run on the raw,

unfiltered eCAP recordings where the 10 kHz artifact was most readily apparent. First, the rolling standard deviation (window size = 250 samples, ~100 ms) was calculated from the raw signal following each LF-VNS pulse. The window size of 250 samples was selected to flatten the standard deviation calculated around the relatively brief LF-VNS stimulation artifact whereas the constant 10 kHz artifact after HF started was unaffected. Next, we compared the maximum value of the rolling standard deviation array for each pulse to a threshold calculated as 3.5X the mean of the standard deviation during the starting portion of the pre-HF period of LF-VNS stimulation which excluded pulses that could have possibly had an HF start(e.g. the first 15s of the pre-HF period when the delay for HF starting was 20s). Pulses without the HF artifact had a low maximum value as both transient artifacts and slow drift were minimized by the rolling window, whereas pulses with HF had a high maximum value corresponding to a 250-sample window containing the 10 kHz HF artifact.

EMG$_{CA}$ Analysis: After identifying the start and end of the HF signal in each trial, the filtered EMG data for a given LF-VNS/HF amplitude combination was sub-divided into pre-HF LF-VNS, during HF (LF-VNS + 10 kHz HF), and post-HF LF-VNS periods (Methods Figure 1B). For quantifying the effect of HF on evoked muscle activity, the root-mean-square (V_{rms}) of the stimulus-triggered average EMG_{CA} signal from each period was calculated with integration windows set to encompass the evoked muscle activity. This window was determined for each pig separately by plotting the EMG_{CA} for each muscle at the maximum LF-VNS amplitude (1 mA) tested in the EMG trials and selecting a window which excluded the LF-VNS stimulation artifact while fully encompassing the muscle response. We selected this approach rather than using the full EMG_{CA} recording to isolate the evoked response from activity induced by the HF signal (see HF Onset Effects). The V_{rms} of the during-HF and post-HF periods were normalized ($\tilde{V}_{rms}$) within trial using the V_{rms} of the pre-HF period to account for subject-to-subject anatomical and experimental preparation differences using the equation (1):

$$\tilde{V}_{rms} = \frac{during\ HF\ V_{rms}}{pre\ HF\ V_{rms}}. \quad (1)$$

eCAP Analysis: The eCAP analyses were performed in a similar manner to the EMG by separating data into pre-HF, during-HF, and post-HF periods. In some subjects (n = 3/5), a large capacitive stimulus artifact was present at high amplitudes that persisted into the eCAP signal. To remove this artifact, the eCAP recordings in these subjects were re-referenced against another channel on the recording array *post-hoc.* The V_{rms} of stimulus-triggered averages from each HF period were then used to quantify the effects of HF on neural conduction with integration windows selected based on individual eCAP components. Integration windows were manually selected based on the phases/lobes of the eCAP signal. The V_{rms} of the during-HF and post-HF periods were normalized within trial against the pre-HF period and used to generate dose-response curves as in the EMG analysis.

To address potential EMG contamination of eCAP component 3 (components 1 and 2 had shorter latency than any EMG artifacts) two approaches were taken. First, the number and latencies of eCAP components were characterized using eCAP recordings taken under paralytic allowing us to confirm that eCAP component 3 was neural in origin by removal of EMG signal sources. This allowed clear identification of component 3 the '+10 kHz HF' periods in trials without paralytic if the HF amplitude was above the EMG block threshold, as identified by the absence of evoked EMG during HF. Secondly, in some subjects, high LF-VNS amplitudes activated the superior laryngeal (SL) nerve which is located cranial to the location of the LF-VNS cuff and innervates both the CA and CT muscles. Activation of this pathway as opposed to the standard conduction path (via the recurrent laryngeal nerve) is distinguishable by the presence of a shorter latency EMG component[5]. As this pathway is due to current escape cranial to the LF-VNS cuff and not propagation down the VN through the HF cuff, the application of HF would not be expected to block muscle activation from the SL and EMG contamination of the eCAP signal could not be ruled out. Thus, component 3 eCAP data were excluded from analyses when this short-latency component was present in the eCAP (P01, P04).

HR (bpm) Analysis: A stimulus-triggered TTL-pulse provided synchronization of LF-VNS with the physiologic recordings from the ADI system. HR was calculated from the raw ECG, pulse, and blood pressure (in pigs where arterial BP was collected via femoral catheter) using the built-in 'Rate' functions of ADI's LabChart software. The ECG-derived HR was used for analysis except in subject P02 where the HF signal introduced a significant artifact into the ECG which interfered with the ADI's rate calculation. To account for differential HR

responses across subjects to LF-VNS (i.e. subjects exhibiting larger bradycardic responses) we assessed the effect of HF on the LF-VNS response by normalizing the change in HR of the during-HF period by the pre-HF period using the equation (2):

$$HF\ Normalized\ dHR = \frac{(HR_{BL} - HR_{HF})}{(HR_{BL} - HR_{pre-HF})} = \frac{dHR_{HF}}{dHR_{pre-HF}}$$

Where $dHR_{pre\text{-}HF}$ is the maximum deflection from baseline (HR_{BL}) over the last 10 s of the pre-HF, LF-VNS only period and dHR_{HF} is the maximum deflection from baseline of the last 10 s during-HF. Baseline was defined as the mean HR during the 10 s prior to initiation of the pre-HF, LF-VNS pulse-train. The last 10 s of each period was used to allow the respective LF-VNS and HF cardiac effects to fully develop given the slower response time of HR to LF-VNS/HF signals. Using this method, a value close to 1 indicates that the HF had little to no effect on the LF-VNS-evoked cardiac effect whereas a value closer to 0 means that the HF signal returned the HR closer to baseline, and a negative value indicates the HR during HF was higher than baseline.

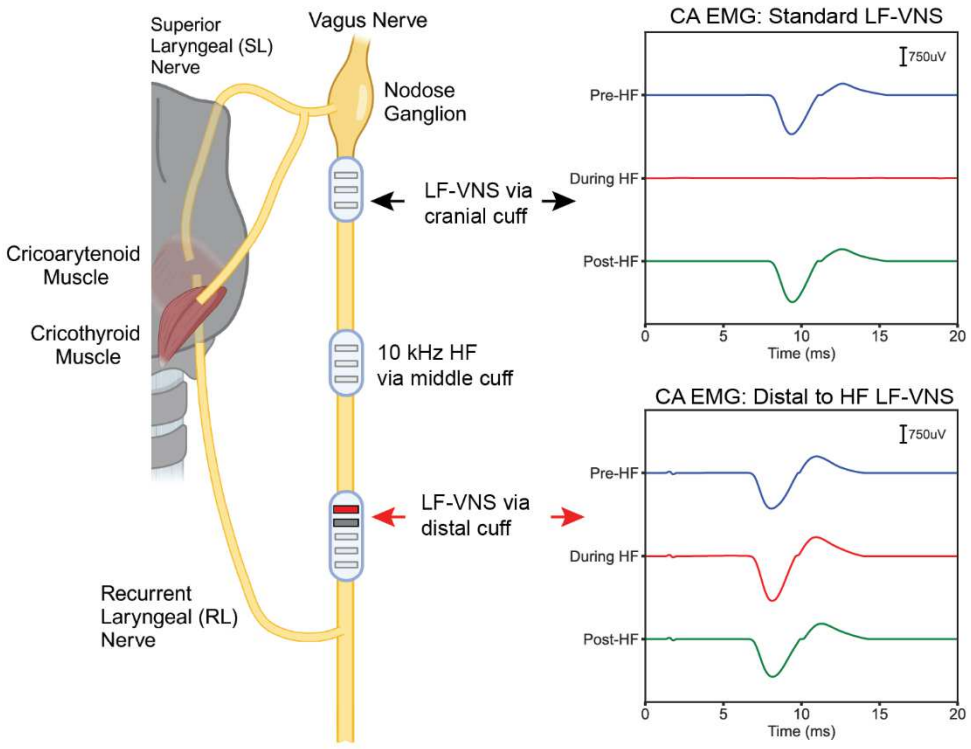
HF Onset Effects: To quantify HF onset effects, we analyzed the entire EMG_{CA} signal during HF. We only analyzed onset responses using EMG data, not eCAP data, because (1) the magnitude of the HF artifact relative to the EMG signal was much smaller and easier to filter, and (2) HF evokes asynchronous activity which is not amenable to stimulus-triggered averaging for improvement of signal-to-noise ratio nor determination of conduction velocities (fiber-types) based on latency. Filtered EMG_{CA} data was plotted using a rasterized format where each row on the y-axis corresponds to a LF-VNS pulse, the x-axis represents time relative to the LF-VNS pulse, and the amplitude of the EMG was denoted by mapping the peak-to-peak EMG signal onto a color axis (Results Figure 4; Supplemental Figures 5, 6). This approach enabled visualization of the pulse-by-pulse effect of HF and evoked asynchronous activity. We applied a simple peak finding algorithm (SciPy, 'find-peaks') with parameters set to detect peaks whose amplitude was >10% of the LF-VNS evoked EMG signal. We then quantified the onset response as the total number of twitches during HF and their magnitude relative to the LF-VNS-evoked twitch (peak-to-peak voltage, not V_{rms}).

Statistical Tests: All statistical tests were performed in Python using the SciPy.stats library. For EMG and eCAP data, statistical tests were run on the normalized data from the HF period relative to the pre-HF LF-VNS evoked signal. To assess the effects of HF on the LF-VNS evoked EMG and eCAP, the non-parametric Kruskal-Wallis test was run on the normalized data (during-HF vs. pre-HF) from all subjects organized by HF amplitude. This test was followed by the non-parametric pairwise Dunn's test where the lowest HF amplitude applied (0.5 mA in all subjects) served as the control group against which every other HF amplitude was tested. To account for multiple comparisons, adjusted p-values were calculated using the Holm-Sidak correction. Correlation between the eCAP and EMG data was performed by calculating the non-parametric Spearman's correlation coefficient function built into the SciPy.stats library.

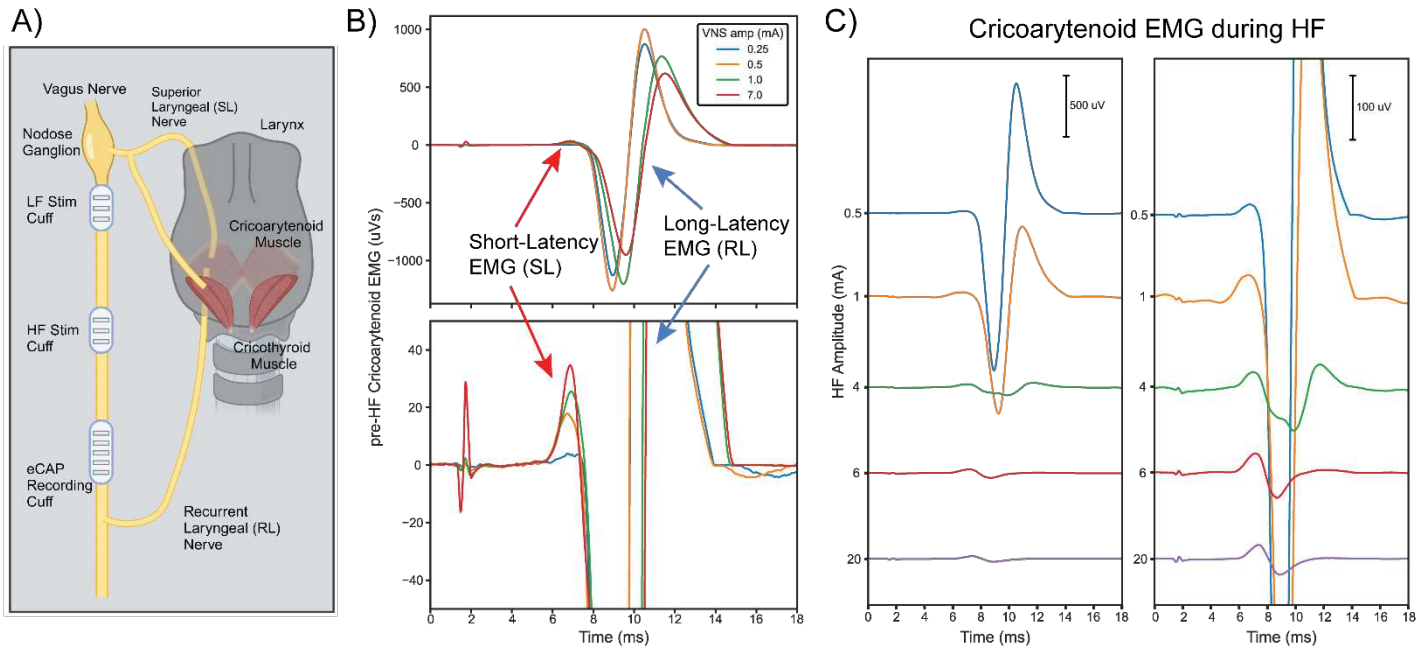
Methods References

1. Pelot, N. A. & Grill, W. M. In vivo quantification of excitation and kilohertz frequency block of the rat vagus nerve. *J. Neural Eng.* **17**, 026005 (2020).
2. Franke, M., Bhadra, N., Bhadra, N. & Kilgore, K. Direct current contamination of kilohertz frequency alternating current waveforms. *Journal of Neuroscience Methods* **232**, 74–83 (2014).
3. Peña, E., Pelot, N. A. & Grill, W. M. Quantitative comparisons of block thresholds and onset responses for charge-balanced kilohertz frequency waveforms. *J. Neural Eng.* **17**, 046048 (2020).
4. Blanz, S. L. *et al.* Spatially selective stimulation of the pig vagus nerve to modulate target effect versus side effect. *J. Neural Eng.* **20**, 016051 (2023).
5. Nicolai, E. N. *et al.* Sources of off-target effects of vagus nerve stimulation using the helical clinical lead in domestic pigs. *J. Neural Eng.* **17**, 046017 (2020).
6. Gasser, H. S. & Erlanger, J. THE RÔLE PLAYED BY THE SIZES OF THE CONSTITUENT FIBERS OF A NERVE TRUNK IN DETERMINING THE FORM OF ITS ACTION POTENTIAL WAVE. *American Journal of Physiology-Legacy Content* **80**, 522–547 (1927).

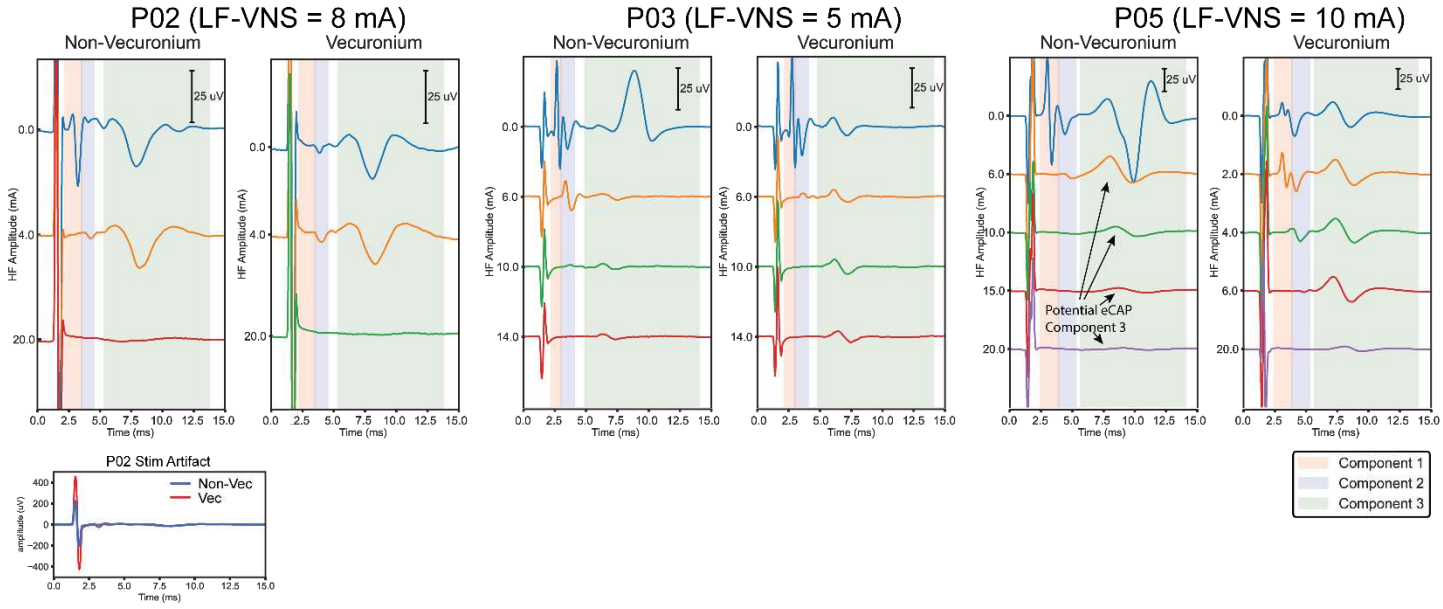
SUPPLEMENTAL FIGURES



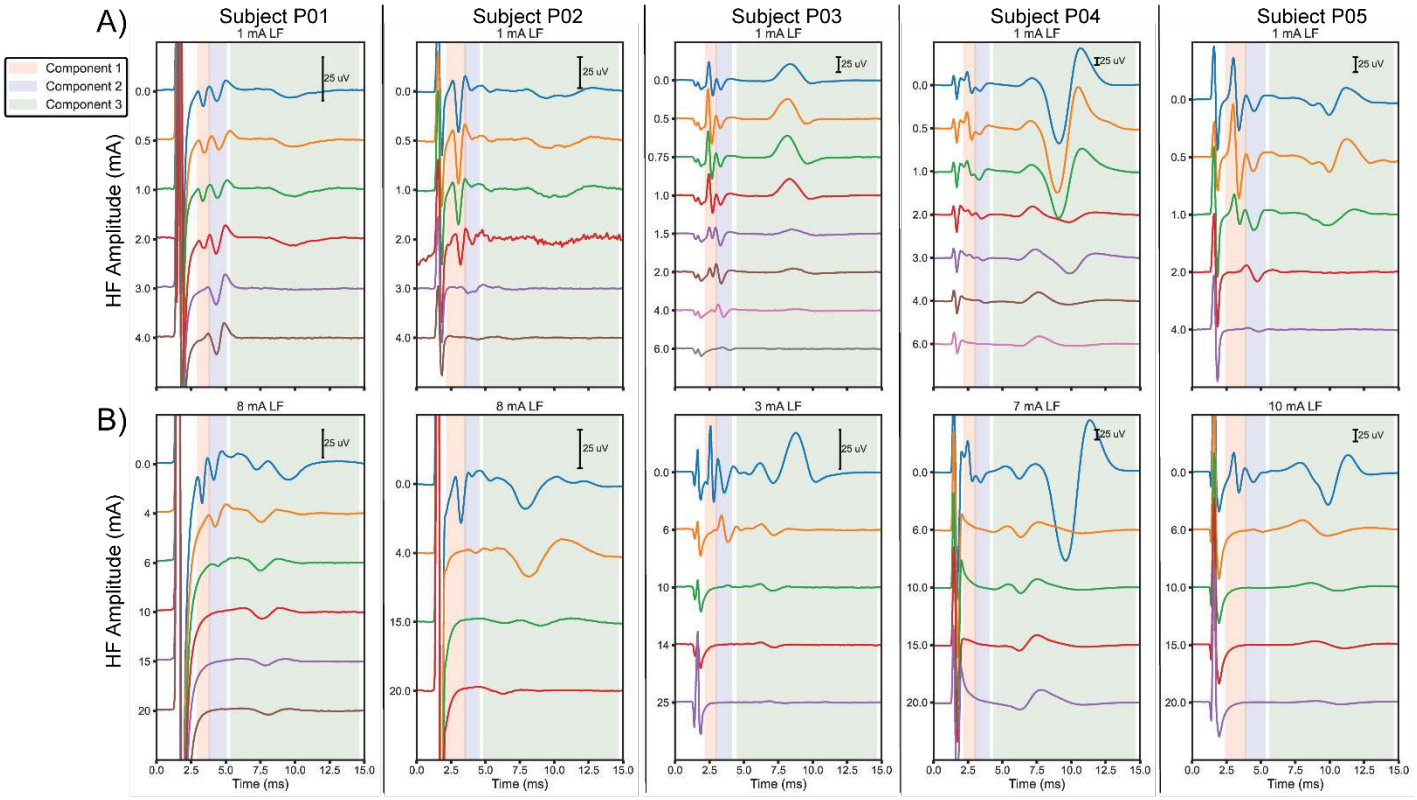
Supplemental Figure 1: Application of 10 kHz high frequency (HF) block at a cranial location does not prevent downstream caudal activation of low-frequency vagus nerve stimulation (LF-VNS) evoked cricoarytenoid (CA) electromyogram (EMG_{CA}). When LF-VNS was applied through the standard (cranial) cuff the evoked EMG_{CA} was completely blocked at this amplitude of HF (4 mA, upper plot). When LF-VNS was applied through the caudal cuff (typically used for recording in these experiments), the evoked EMG_{CA} was completely unaffected by the same amplitude of HF (lower plot). Subject P05.



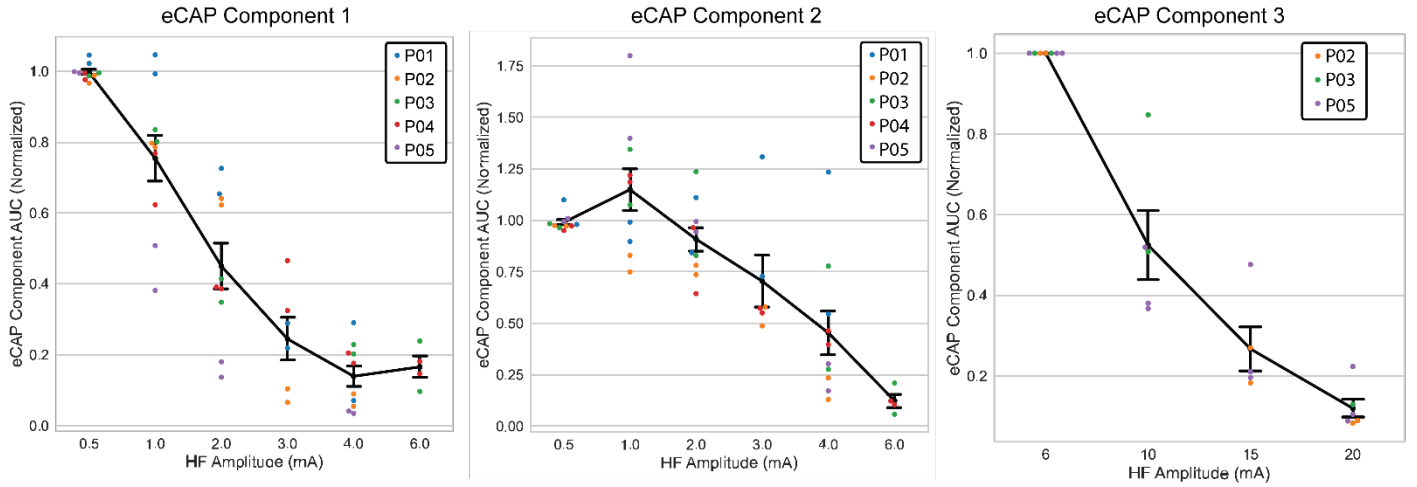
Supplemental Figure 2: High-frequency (HF) block of low-frequency vagus nerve stimulation (LF-VNS) evoked electromyogram (EMG) was limited to conduction through the recurrent laryngeal (RL) mediated pathway. **A)** Anatomic schematic of neck muscles innervated by the vagus nerve (VN). The cricoarytenoid (CA) muscle is innervated by the RL which branches from the VN caudal to the LF-VNS, HF, and evoked compound action potential (eCAP) cuffs. Conversely, the superior laryngeal (SL) nerve branches off cranial to the cuffs at the nodose ganglion and innervates both the CA and cricothyroid (CT) muscles. The SL can be activated by LF-VNS from a stimulation cuff placed ~1 cm caudal to the nodose ganglion due to current escape at high LF-VNS amplitudes or from a poorly insulated cuff. **B)** Activation of the SL and RL pathways can be distinguished by the latency of the evoked EMG_{CA} where the SL (red arrows) evokes a shorter latency response than the RL pathway (blue arrows, subject P04). **C)** Evoked EMG_{CA} responses to increasing doses of HF in an experimental trial where the SL pathway was activated. (Left) Full view of the LF-VNS-evoked EMG_{CA} during 1 mA LF-VNS; as the HF amplitude was increased, the larger and slower latency RL-mediated response was blocked by 4 and 20 mA HF whereas a smaller and shorter latency SL-mediated response was unaffected by the HF signal. (Right) Re-scaled (zoomed in) view of the same data.



Supplemental Figure 3: Confirmation of evoked compound action potential (eCAP) Component 3 with a muscle paralytic (vecuronium bromide). eCAP recordings in response to specified LF-VNS at increasing levels of HF from subjects in which this control was performed (n = 3/5). Due to the slower conduction velocity (longer latency) of small diameter fibers, their eCAPs are often contaminated by electromyogram (EMG) signals. As the LF-VNS-evoked EMG was blocked by increasing amplitudes of HF, we suspected that the residual signal in the eCAP recordings at these amplitudes was a true neural eCAP component that reflected activation of small diameter fibers and their subsequent block at very high HF amplitudes. To confirm that Component 3 was neural in origin, we repeated a subset of trials with a muscle paralytic (vecuronium bromide) in the subjects shown here. Note, in P02 there was a substantial difference in the stim artifact of the eCAP (lower plot) indicating a change in the experimental preparation's status (i.e. stim/recording cuff electrode conformance, edema within the pocket, movement of cuff over day, etc.,) between the non-vecuronium and vecuronium trials resulting in differences between them in the pre-HF period (HF = 0 mA).

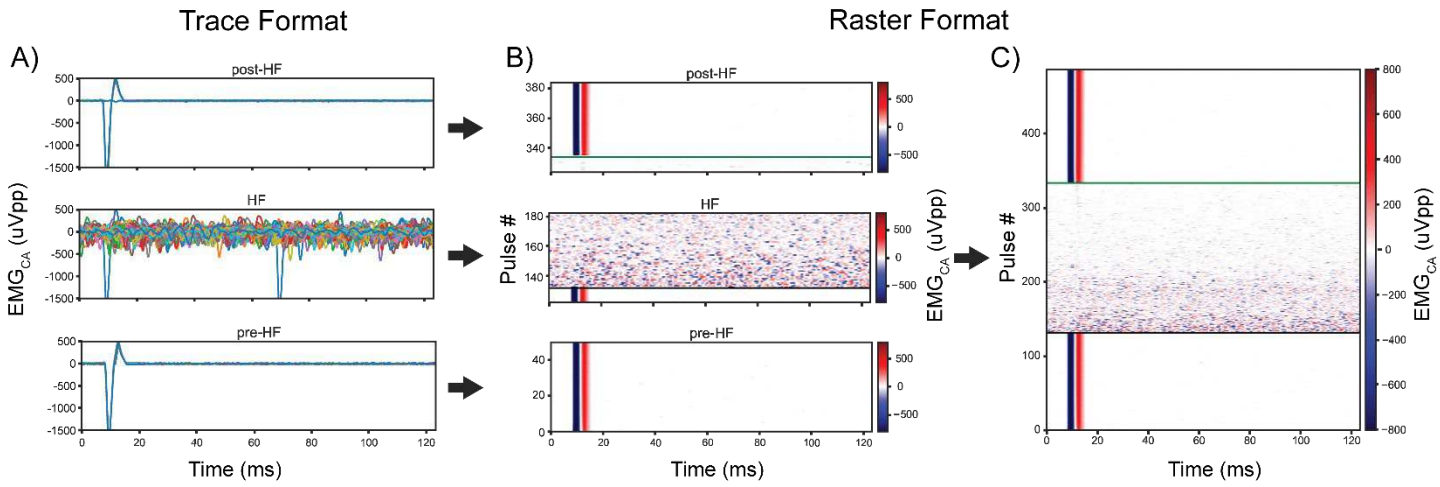


963

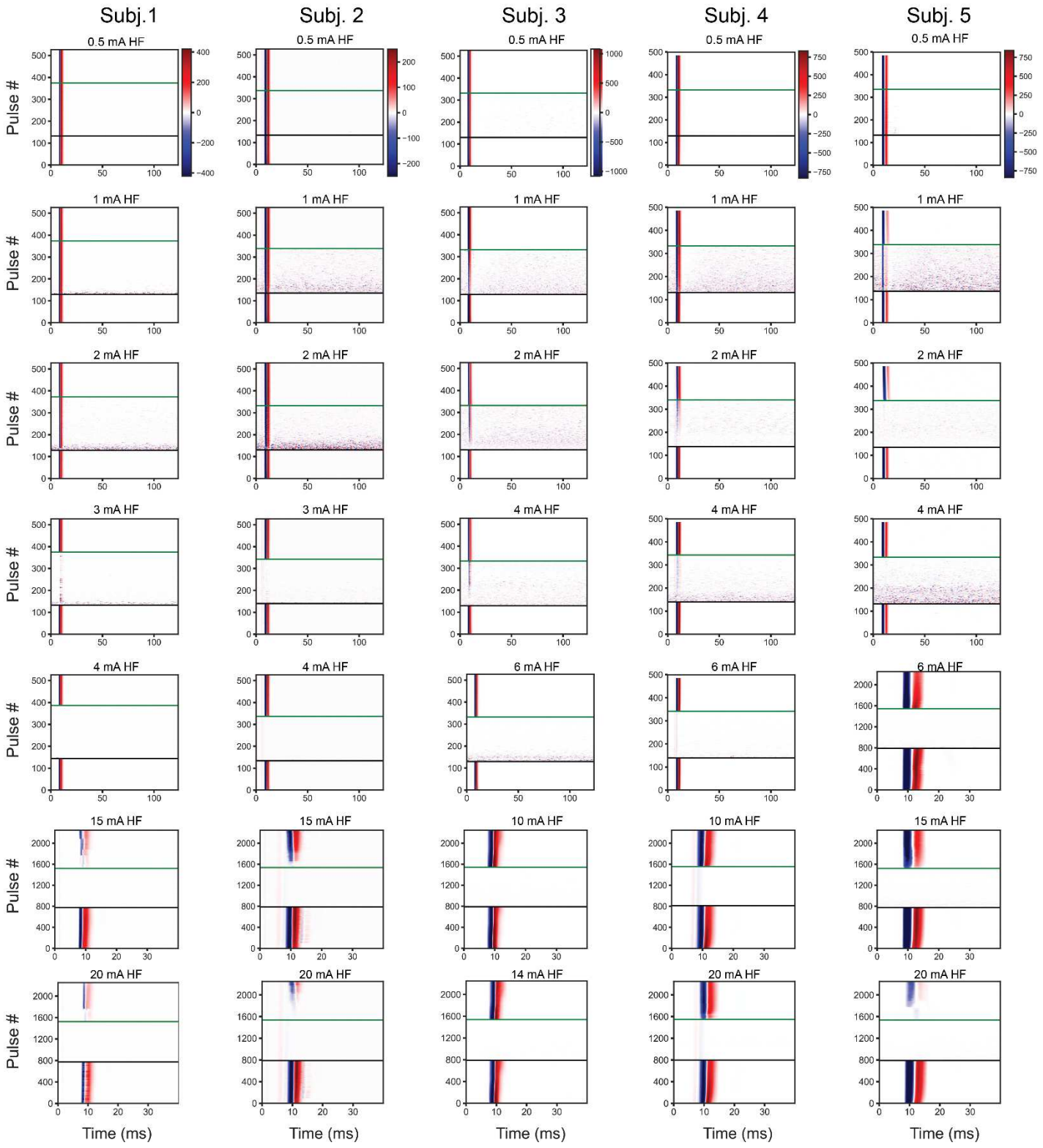


964

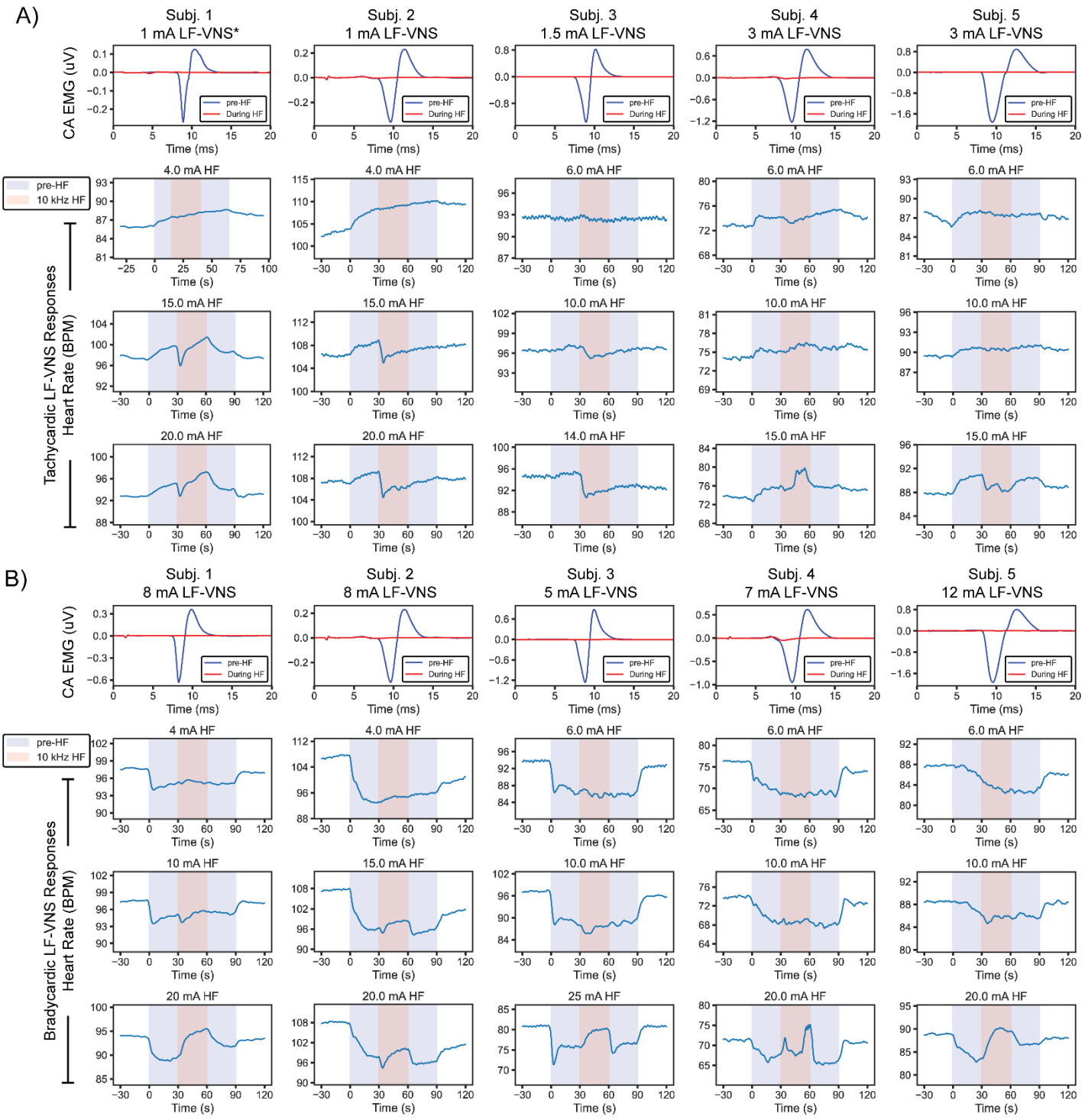
965 Supplemental Figure 4: Individual subject neural (eCAP) responses to LF-VNS and HF. **A,B)** Stimulus-triggered
966 average of the evoked compound action potential (eCAP) elicited by specified levels of LF-VNS with increasing
967 HF amplitudes. **C)** Cohort dose-response curve of specified eCAP components with individual responses
968 shown. For components 1 & 2, data were normalized within trial against the pre-HF (LF-VNS only) period. For
969 component 3, data were normalized against the HF period at HF = 6 mA as this was shown to block the LF-
970 VNS-evoked EMG_{CA} and remove EMG contamination from the eCAP signal (see main text Figure 2). Subjects
971 (P01, P04) which exhibited short-latency (superior laryngeal mediated) EMG responses contaminating the
972 eCAP recordings were also excluded from eCAP 3 analysis.



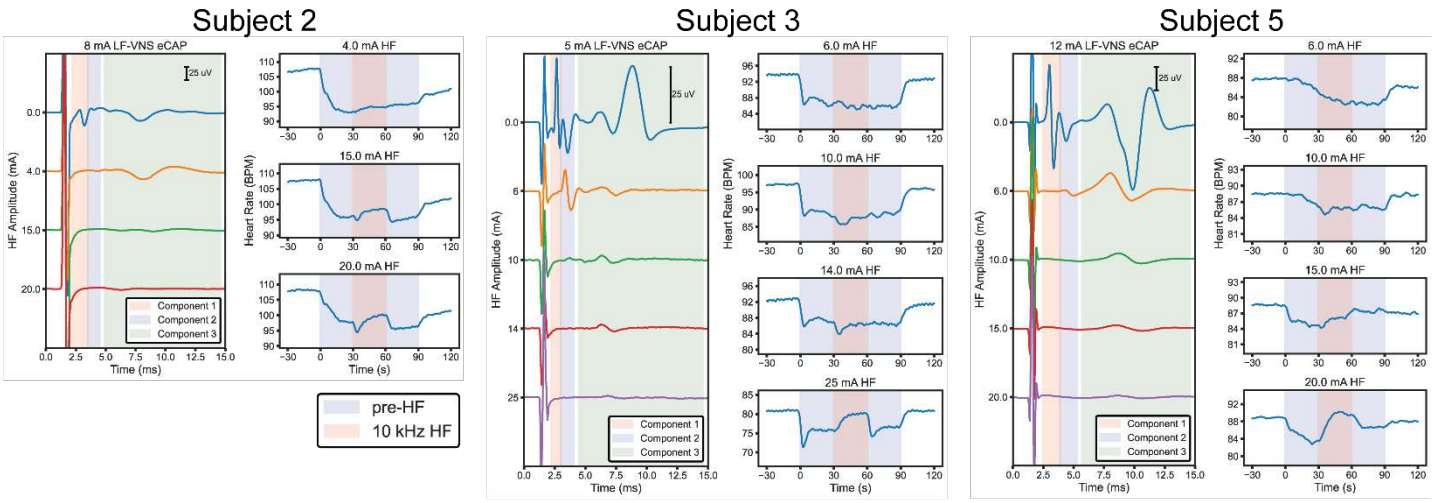
Supplemental Figure 5: Process to rasterize the electromyogram (EMG) responses to high-frequency (HF) signals. **A)** The standard format for displaying EMG responses to electrical stimulation is by plotting the EMG's voltage trace in a 2D format where the x-axis is time post-stimulus and the y-axis is the measured EMG voltage. These example time series data depict the cricoarytenoid EMG (EMG_{CA}) response to 1 mA low-frequency vagus nerve stimulation (LF-VNS) with 4 mA HF. The first 50 EMG_{CA} voltage traces from each of the different phases (pre-HF, with HF, and post-HF) of the trial are superimposed and plotted from the bottom to top rows. While this format provides visualization of the LF-VNS-evoked EMG_{CA} twitch (the consistent spike in the pre- and post-HF plots at t = ~10 ms), the superposition of the EMG_{CA} traces during HF makes visualization and interpretation difficult as the irregular HF-evoked activity causes the overlaid traces to become an indistinguishably noisy signal. Further, if these traces underwent stimulus-triggered averaging, the asynchronicity of the HF-evoked activity may cause it to be averaged out completely and appear as though HF blocked the LF-VNS evoked EMG_{CA} without any other effects. **B)** To better visualize the effect of HF, we plotted the data using a rasterized format where the y-axis is LF-VNS pulse number and the EMG_{CA} voltage is represented by a color-axis. These example raster plots depict the same fifty traces as in (A). The black lines in the 'HF' and green line in the 'post-HF' plots denote the start and end of HF, respectively. The consistent LF-VNS-evoked EMG_{CA} twitch is seen in the dark blue/red bands with the same latency as the trace format, at t = ~10 ms (B, bottom/top rows). In this trial, the 4 mA HF immediately and completely blocked the LF-VNS evoked twitch; however, it simultaneously evoked asynchronous EMG_{CA} responses as evidenced by the randomly distributed colored dots following the onset of HF (B, middle row). Interestingly, the magnitude of these twitches (the darkness of the dots) is considerably less than the LF-VNS evoked twitch and decreases over the duration of HF. **C)** Depicts the rasterized format of all pulses from the trial shown in panels A and B, rather than only the first 50 pulses of each period. The asynchronous EMG_{CA} activity only occurs during the first half of HF while block of the LF-VNS-evoked EMG_{CA} twitch is maintained during the HF period and immediately recovers following end of HF.



Supplemental Figure 6: Rasterized cricoarytenoid electromyogram (EMG_{CA}) responses to low-frequency vagus nerve stimulation (LF-VNS, 1 mA all plots) and increasing high-frequency (HF) amplitudes across study cohort. Black lines denote start of HF and green lines denote end of HF. Color represents peak-to-peak amplitude (μV_{pp}) of the EMG_{CA} signal plotted as a function of time and LF-VNS pulse number.



Supplemental Figure 7: Demonstration of the 'HF-window' across the cohort, wherein the EMG_{CA} response is blocked while the HR response is maintained. In all subjects, we found that the high-frequency (HF) amplitude necessary to block low-frequency vagus nerve stimulation (LF-VNS) evoked cricoarytenoid electromyogram (EMG_{CA}) was below the threshold at which HF affected the LF-VNS cardiac response (to both (A) tachycardic and (B) bradycardic responses). The top row of panels A and B shows the paired LF-VNS evoked EMG_{CA} response before (blue trace) and during (red trace) HF stimulation (HF amplitude of EMG_{CA} plot = HF amplitude of first HR plot). The other three rows in panels A and B show the cardiac effects at the same level of LF-VNS with increasing HF amplitude. Note that HF-evoked cardiac effects are generally absent in the topmost cardiac traces; as HF amplitude is increased, HF-evoked cardiac effects are apparent by the rapid change in heart rate trajectory at the onset of HF (red shaded region).

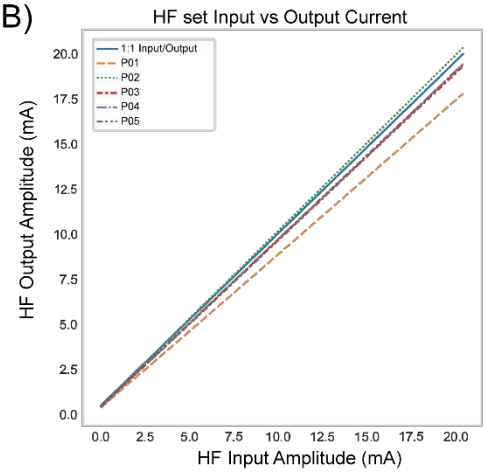


Supplemental Figure 8: Relationship between evoked compound action potential (eCAP) Component 3 and high-frequency (HF) effects on the low-frequency vagus nerve stimulation (LF-VNS) cardiac response. Given the limited datapoints, variability in the LF-VNS/HF responses at high LF-VNS and HF amplitudes across subjects, and the presence of short-latency (superior laryngeal-mediated) EMG contamination in subjects P01 and P04, a direct correlation between eCAP component 3 and the effect of HF on the LF-VNS cardiac response across the study cohort was not feasible. However, visual assessment of eCAP Component 3 and paired cardiac responses in subjects P02, P03, and P05 appear to show a linear relationship between HF block of Component 3 and HF block of LF-VNS bradycardic effects, suggesting that eCAP Component 3 represents small diameter vagal cardiac efferents. Subject 3: Trial with HF amplitude of 25 mA, LF-VNS amplitude was 7 mA.

A)

Input HF Amplitude (mA)	Measured HF output (mA)					Cohort	
	P01 ‡	P02 ‡	P03	P04	P05	Average HF output (mA)	% of Input Amplitude
0.5	0.38	0.42	0.4	0.41	0.43	0.41	81.60
0.75					0.68	0.68	90.67
1	0.83	0.93	0.89	0.91	0.92	0.90	89.60
1.5			1.39			1.39	92.67
2	1.74	1.95	1.88	1.9	1.91	1.88	93.80
3	2.6	2.98		2.86		2.81	93.78
4	3.49	4.01	3.8	3.82	3.84	3.79	94.80
6	5.27	6.06	5.73	5.78	5.78	5.72	95.40
7			6.31			6.31	90.14
8	7.05	8.09	7.68			7.61	95.08
10	8.84	10.13	9.62	9.68	9.68	9.59	95.90
15	13.32	15.24		14.5	14.55	14.40	96.02
20	17.8	20.35	19.33	19.45	19.43	19.27	96.36
30		30.14	25.97			28.06	93.52
40		40.16	34.82			37.49	93.73
60			52.49			52.49	87.48

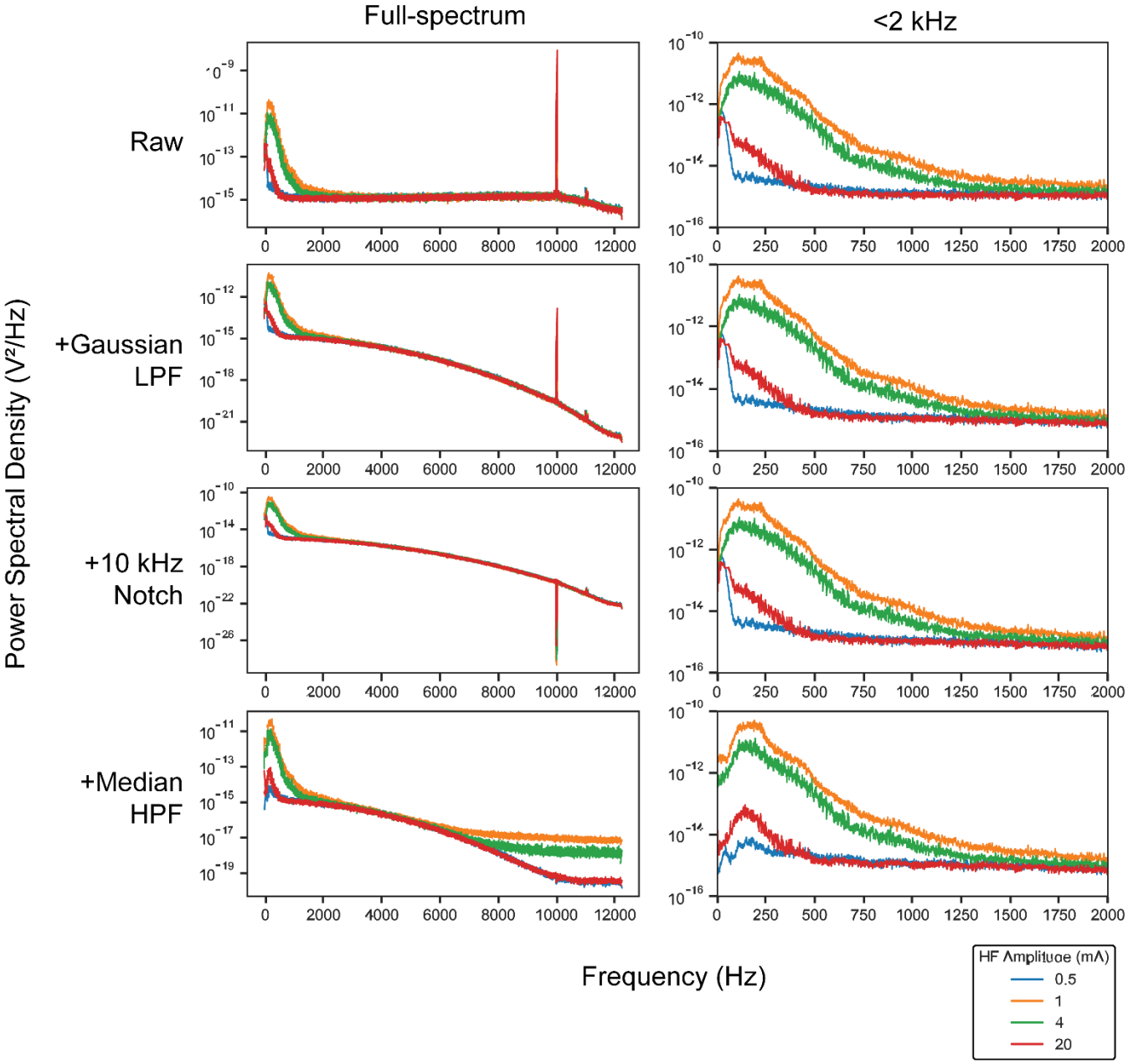
B)



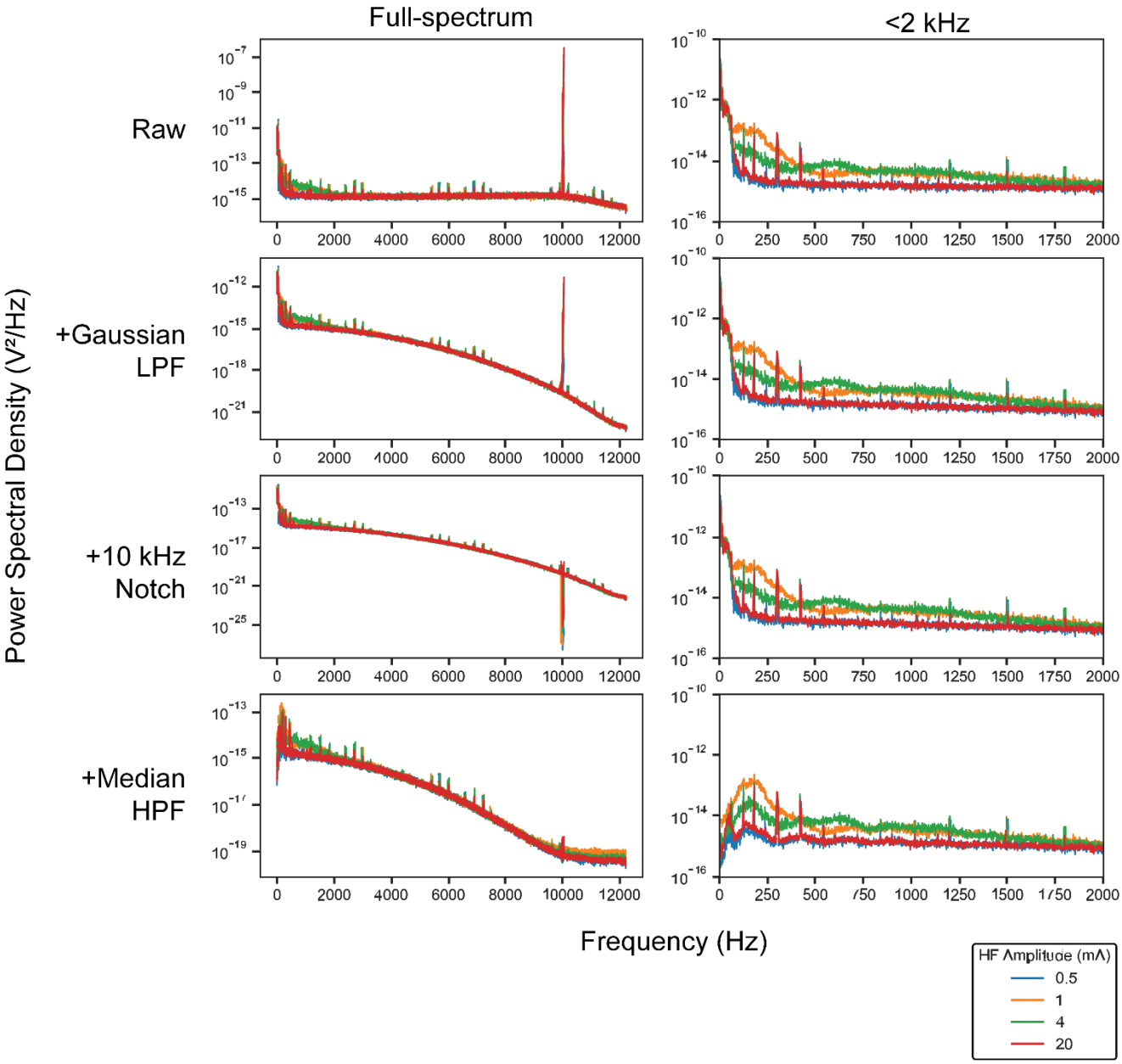
C)

	HF Stim/Record Setup
P01	HF via single Keithley 6221. Current output recorded by TDT ADC
P02	HF via 5 Keithley 6221's with synchronized triggers. Current output recorded by TDT ADC
P03	HF via single Keithley 6221 into AM-Systems4100. Current output recorded by Keithley 6510.
P04	HF via single Keithley 6221. Current output recorded by Keithley 6510
P05	HF via single Keithley 6221. Current output recorded by Keithley 6510

Supplemental Figure 9: Comparison of the specified high-frequency (HF) stimulation current versus the measured output across experimental cohort. Due to concerns about attenuation of the 10 kHz HF signal, the voltage across an in-series 100 Ω resistor was measured and used to compare the applied HF current against the specified current amplitude. A) Table showing the HF current measured based on the input HF amplitude, grayed out boxes are amplitudes which were not tested in that subject. ‡: In P01 and P02, the HF output was measured using the TDT's onboard ADC which attenuated the actual amplitude due to a hardware low-pass filter. Thus, output current levels represent a post-hoc calculated output based on benchtop testing. B) Plot shows the relationship of input to output up to 20 mA input HF amplitude. C) Table showing differences in the HF stimulation/measurement hardware across subjects.



Supplemental Figure 10: Filtering 10 kHz artifact. Power spectral density (PSD, Welch's method) plots of the cricoarytenoid electromyogram (EMG_{CA}) from trials with only high-frequency (HF) stimulation (no LF-VNS) at 0.5 to 20 mA. PSD of the raw data (top row) shows a significant HF artifact that scales with the HF amplitude. To remove this artifact, we first applied a Gaussian low-pass filter (sigma = 1.29) followed by a 10 kHz notch filter. A subsequent median high-pass filter (kernel = 201) was then applied to address baseline drift. The right column shows the PSD at frequencies < 2 kHz which contains the range at which EMG_{CA} is expected to be present (0 – 500 Hz). The effect of the HF-evoked asynchronous activity can be seen in the larger low-frequency power at 1 and 4 mA HF. Notably, if the asynchronous activity in the EMG_{CA} signal was a signal processing artifact created by filtering of the HF signal, it would be expected to increase with HF amplitude. Instead, the low-frequency power at 20 mA HF is closer to 0.5 mA HF in both the raw and filtered signals. Across the cohort, 0.5 mA HF did not evoke asynchronous EMG_{CA} activity whereas at 20 mA, the effect of HF on the motor fibers was almost immediate and minimal asynchronous activity was observed (see Raster plots, Supplemental Figure 5).



Supplemental Figure 11: Power spectral density (PSD) of the evoked compound action potential (eCAP) with filtering approach. Data are from the same HF-only trials as Supplementary Figure 10. Spikes in PSD are harmonics of 60 Hz powerline noise. Although we did not specifically filter out powerline noise (or its harmonics), it was averaged out of our eCAP analyses by using stimulus-triggered averaging and a low-frequency vagus nerve (LF-VNS) stimulation frequency that is not an even multiplier of 60 Hz (i.e. 8.1 and 25 Hz).